Pergamon

Int. J. Solids Structures Vol. 35, No. 17, pp. 2121–2149, 1998

0020-7683/98 $19.00 + .00

PII: S0020-7683(97)00168-6

LINEAR ELECTRO-ELASTIC ANALYSIS OF A CAVITY OR A CRACK IN A PIEZOELECTRIC MATERIAL

TONG-YI ZHANG, CAI-FU QIAN and PIN TONG
Department of Mechanical Engineering, Hong Kong University of Science the Technology, Clear Water Bay, Kowloon, Hong Kong
E-mail: mezhangt@usthk.ust.hk

(*Received* 22 *October* 1996; *in revised form* 26 *May* 1997)

Abstract—Analytical solutions for an elliptical cylinder cavity or a crack inside an infinite piezoelectric medium under combined mechanical–electrical loadings are formulated via the Stroh formalism and well confirmed by finite element analysis. The results show that the stress and electric fields in the vicinity of the crack tip are, in general, determined by a complex vector of intensity factors. The complex vector of intensity factors may reduce to be real under certain circumstances. For a vacuum crack, the electric field inside the crack in the direction perpendicular to the crack magnifies the corresponding applied electric field by more than 1000 times. In this case, the electric field strength in the material has a finite value at the crack tip, but the electric displacement approaches infinity at the crack tip due to the piezoelectricity. The self-consistent analysis is developed to determine the deformed crack profile. The energy release rate for the cavity propagation is formulated under the condition that the ratio of the minor semi-axis to the major semi-axis of the ellipse remains unchanged. For an insulating crack, the applied electric field contributes nothing to the energy release rate when the undeformed crack profile is used, while the electric field resists crack propagation when the deformed crack profile is used. For a conducting slit crack, the energy release rate is independent of the applied electric field perpendicular to the crack, and is enhanced by the applied electric field parallel to the crack. © 1998 Elsevier Science Ltd.

1. INTRODUCTION

The mechanical reliability of piezoelectric materials becomes increasingly important as they are used in more and more sophisticated areas. Thus, there has been tremendous interest in studying the fracture behavior and fracture mechanics of those materials (Barnett and Lothe 1975; Pohanka *et al.*, 1976; Pohanka *et al.*, 1978; Cherepanov, 1979; Deeg, 1980; Yamamoto *et al.*, 1983; Pak and Herrmann 1986; McMeeking, 1989; Mehta and Virkar, 1990; Pak, 1990, 1992; Sosa and Pak, 1990; Suo *et al.*, 1992; Zhang and Hack, 1992; Suo, 1993; Kumar and Singh, 1996; Lynch, 1996a; Zhang and Tong, 1996; Hom *et al.*, 1996; Kumar and Singh, 1997a, b). However, there is still confusion regarding the effect of electric field on the fracture behavior and criterion. For the case that a crack is treated as a mathematics slit without any thickness and has a finite dielectric constant, the energy release rate for crack propagation evaluated from linear fracture mechanics is positive definite and independent of applied electric fields when the electric field inside the crack is considered (McMeeking, 1989; Zhang and Tong, 1996). On the other hand, the energy release rate is not positive definite and the electric loading would always impede crack propagation if the electric field inside the crack is ignored (Pak, 1990; Suo *et al.*, 1992). Experimentally, significant differences in the crack growth behavior perpendicular and parallel to the poling direction of PZT ceramics were observed by Yamamoto *et al.* (1983), Mehta and Virkar (1990) and Tobin and Pak (1993) in indentation fracture tests under static and time-varying electric loadings. For a given mechanical load, a positive electric loading increases the crack length normal to the poling axis, while a negative electric loading reduces it. Park and Sun (1995) carried out mode I and mixed mode fracture tests on PZT-4 piezoelectric ceramics and observed that a positive electric field tends to open the crack and reduce the fracture load while a negative electric field increases it. Those experimental results cannot be explained if the energy release rate derived from linear fracture mechanics is used as a fracture criterion regardless of whether the crack is treated as being electrically permeable

or not. To solve this problem, Park and Sun (1995) argued that the fracture process is mechanical in nature and, therefore, only the mechanical energy release rate should be used as a fracture criterion, which linearly depends on the applied electric field. Recently Gao *et al.* (1997) proposed, by analogy to the classical Dugdale model, an electric strip saturation model and hence derived the local and global energy release rates. Under small-scale yielding conditions, the global energy release rate is equal to that of a linear piezoelectric crack without electrical yielding. The local energy release rate gives linear predictions which agree with the above-mentioned experimental results. Since it is assumed that the electric yielding zone remains unchanged during crack propagation, only the mechanical energy is taking into account in the local energy release rate. In this sense, the local energy release rate provides a physical basis to the mechanical energy release rate.

Another important issue in studying fracture mechanics of piezoelectric materials is the electric boundary condition along the crack faces. One commonly used boundary condition is the specification that the normal component of electric displacement along the crack faces equals zero (Pak, 1990). This boundary condition ignores the electric field within the crack. The other commonly used boundary condition treats the crack as being electrically permeable (Mikhailov and Parton, 1990). Sosa (1991) has investigated the mechanical and electrical fields in the vicinity of circular and elliptical holes and used the asymptotic expressions for the electromechanical fields in the vicinity of a crack to study the electric fields' effects on crack arrest and crack skewing (Sosa, 1992), Pak and Tobin (1993) found the ratio of the crack tip electric field to the applied field approaches unity as an elliptical cavity reduces to a slit. Dunn (1994) also investigated the effects of crack face boundary conditions on the energy release rate in piezoelectric solids. His results indicate that the impermeable assumption can lead to significant errors regarding the effects of the electric fields on crack propagation based on an energy release rate criterion. In a previous paper (Zhang and Tong, 1996), we studied the boundary conditions by investigating an elliptical cylinder cavity. In the limiting process, we found that the two commonly used boundary conditions are actually two extremes of the exact boundary conditions. Since the electric field exists in air and in vacuum, both the geometry and size of the crack have a great influence on fracture behavior of these materials (Zhang, 1994a; Zhang and Tong, 1996). In the present work, we investigate the general behavior of cracks by studying an elliptical cylinder cavity. Only in this way can we determine the electric field within the cavity (crack).

In a real sintered piezoelectric sample, there are many flaws, each having a finite width and finite size, i.e. they are not mathematically slits. Those size effects on the energy release rate have been studied under pure electric loadings (Zhang, 1994a). In this case, letting the crack width approach zero and maintaining the dielectric constant of vacuum as its finite value, 8.85×10^{-12} F/m, where F and m denote, respectively, farad and meter, the electric field will contribute nothing to the energy release rate. On the other hand, the electric field does impeded crack propagation if the crack width has a relatively large value (Zhang, 1994a)†.

The above-mentioned theoretical approaches are on the basis of linear fracture mechanics. However, real piezoelectric materials behave nonlinearly, in particular, under high level of applied electric and/or mechanical loadings. Jona and Shirane (1993) described in detail the electrical and mechanical properties of piezoelectric crystals. The relationship between strain and electric fields is nonlinear and their hysteresis loop looks like a "butterfly". Cao and Evans (1994) found the mechanical nonlinearity in poled PZT piezoelectrics. Lynch (1996b) studied the nonlinear electro-mechanical response of 8/65/35 PLZT under a compressive uniaxial stress. Those electrical, mechanical and electro-mechanical nonlinearities are induced by electrical domain switching (Jona and Shirane, 1993; Cao and Evans, 1994; Lynch, 1996b). A linear analysis would be valid if a small scale yield assumption is made, e.g. the model of multiscale energy release rates is proposed under such assumption (Gao *et al.*, 1997). In addition, a linear electro-elastic analysis is the first step to understand the fracture behavior of piezoelectric materials. Even at this stage, as

† Equation (7) in the note (Zhang, 1994a) should be corrected as $F = \int V \mathrm{d}Q$ and accordingly eqns (8), (9), (11) and (14) should change the sign.

discussed above, the boundary conditions along the crack faces and the energy release rate should be clarified, which is the goal of the present work.

In the present study, the mechanical and electric fields for a linear anisotropic piezoelectric medium with an elliptical cylinder cavity or a crack under combined mechanical–electric loadings have been systematically formulated in Sections 2 and 3 via the Stroh formalism attached in Appendix 1. In Section 4, the energy release rate for a cavity or crack propagation is given based on the thermodynamic approaches described in Appendix 2. A geometrically nonlinear analysis, called self-consistent calculation, has been developed in Section 5 to determine the deformed crack profile in the presence of a strong electric field inside the crack. In Section 6, examples for a specific material (PZT-4 ceramic) are presented to explicitly demonstrate the analytical result together with some finite element confirmation. Finally, concluding remarks are given in Section 7.

2. SOLUTIONS FOR AN ELLIPTICAL CYLINDER CAVITY

The general solution for the coupled mechanical-electric problem is described in Appendix 1. Now, consider an infinite piezoelectric material containing an elliptical cylinder cavity ($x_1^2/a^2 + x_2^2/b^2 = 1$) under combined mechanical–electric loadings, as shown in Fig. 1, where a and b are, respectively, the major and minor semi-axes of the ellipse. The electric loading is in-plane mode, while the mechanical loading can be in-plane tension and/or shear (mode I and/or mode II), and/or anti-plane shear (mode III). Previous work by the authors (Zhang and Tong, 1996) reports solutions for the in-plane electric and anti-plane mechanical loadings; the present work studies general cases.

The boundary conditions along the surface of an elliptical cavity have the following forms

$$\sigma_\perp = 0 \quad \text{(traction-free)} \tag{1}$$

$$D_\perp = D^c{}_\perp \quad \text{(surface charge-free)} \tag{2}$$

$$E_\parallel = E_\parallel^c \quad \text{(irrotionality of electric fields)} \tag{3}$$

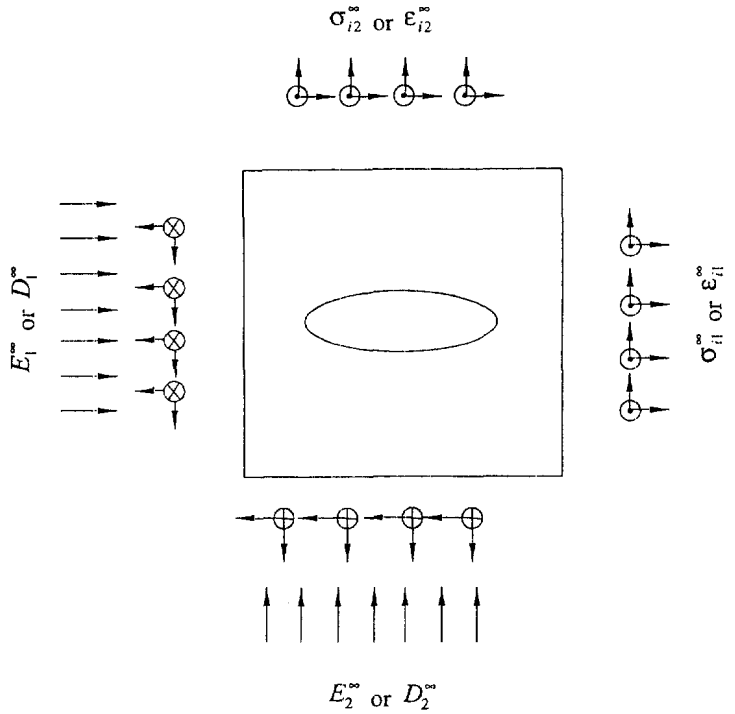

Fig. 1. Remote mechanical and electric loads in the z-plane.

where σ denotes pure mechanical stress; the superscript c refers to "in the cavity", while parameters "in the material" do not have any superscript; and the subscripts $\perp$ and $\|$, respectively mean "perpendicular" and "parallel" to the surface.

Since only an electric field exists in the cavity, the governing and the constitution equations are, respectively, reduced to

$$\nabla^2 \phi^c = 0 \tag{4}$$

$$D_i^c = \kappa^c E_i^c = -\kappa^c \frac{\partial \phi^c}{\partial x_i}, \quad i = 1, 2 \tag{5}$$

where κ^c is the dielectric constant of the cavity and the electric field inside the cavity is treated isotropically. In the present work, κ^c may change from 8.85×10^{-12} F/m for a vacuum cavity to infinity for an electrically conductive cavity. The general solution to eqn (4) is

$$\phi^c = \Phi(z) + \overline{\Phi(z)} \tag{6}$$

where $\Phi(z)$ is a complex analytic function of z with $z = x_1 + ix_2$, and the overbar means complex conjugate. The complex electric field, E^c, and electric displacement, D^c, are, respectively, given by

$$E^c = E_1^c - iE_2^c = -2\frac{d\Phi}{dz}, \quad D^c = D_1^c - iD_2^c = -2\kappa^c \frac{d\Phi}{dz}. \tag{7}$$

In order to determine Φ, we introduce the mapping function

$$z = R\left(w + \frac{m}{w}\right) \tag{8}$$

which maps the ellipse in the z-plane to a unit circle in the w-plane, where $w = v_1 + iv_2$, $R = (a+b)/2$, and $m = (a-b)/(a+b)$. The line segment $(-c, c)$ in the z-plane is mapped to a circle with a radius $\sqrt{m}$ in the w-plane, as shown in Fig. 2, where $c^2 = a^2 - b^2$. The electric field must be single-valued along the linear segment in the z-plane; as such it requires that

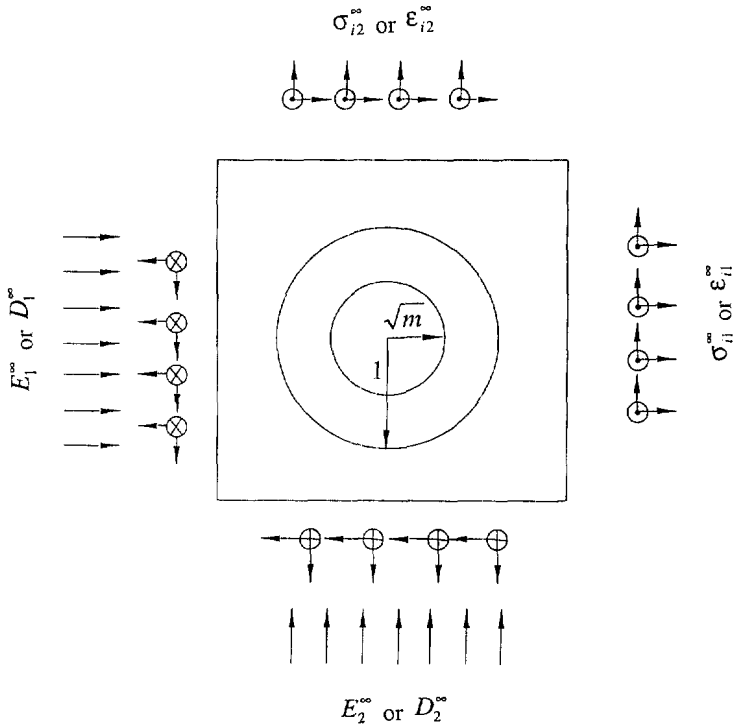

Fig. 2. Mapping the elliptical cavity to a unit circle in the w-plane.

$$\Phi(\sqrt{m}\,e^{i\theta}) = \Phi(\sqrt{m}\,e^{-i\theta}) \tag{9}$$

in the w-plane, where θ is the polar angle. The inverse mapping function of eqn (8) is

$$w = \frac{z+\sqrt{z^2-c^2}}{2R}. \tag{10}$$

The general solution for a piezoelectric material is given by eqns (A14)–(A16) in Appendix 1. In each of the four z_α-planes, where $z_\alpha = x_1 + p_\alpha x_2$ and p_α is the eigenvalues with positive imaginary part (see Appendix 1 for details), the ellipse is distorted. However, the following mapping function

$$z_\alpha = R_\alpha\left(w_\alpha + \frac{m_\alpha}{w_\alpha}\right) \tag{11}$$

can map the four distorted ellipses to a unit circle, where

$$R_\alpha = \frac{a-ip_\alpha b}{2}, \quad m_\alpha = \frac{a+ip_\alpha b}{a-ip_\alpha b}. \tag{12}$$

Similarly, the inverse mapping function has the following form

$$w_\alpha = \frac{z_\alpha+\sqrt{z_\alpha^2-c_\alpha^2}}{2R_\alpha} \tag{13}$$

where

$$c_\alpha^2 = a^2 + p_\alpha^2 b^2. \tag{14}$$

As expected, eqn (13) yields $w_\alpha = e^{i\theta}$ $(-\pi < \theta \leqslant \pi)$, when $z_\alpha = a\cos\theta + p_\alpha b\sin\theta$, i.e. along the elliptical hole surface. Now, the problem in the z-plane can be solved by mapping the elliptical hole to the circular ring in the w-plane. The boundary conditions along the surface of the cavity can be expressed in terms of the extended functions (see Appendix 1 for details)

$$\psi_i = 0, \quad i = 1,2,3 \quad \text{(traction-free)} \tag{15}$$

$$\psi_4 = -i\kappa^e(\Phi - \bar{\Phi}) \quad \text{(surface charge-free)} \tag{16}$$

$$u_4 = \phi^e \quad \text{(irrotationality of electric fields).} \tag{17}$$

Equations (16) and (17) indicate that both electric potentials inside the cavity and the outside medium have the same reference.

The complex potential Φ has the following form

$$\Phi = Rc\left(w + \frac{m}{w}\right) \tag{18}$$

where c is a constant to be determined. The component of vector $\mathbf{f}$ in eqns (A14)–(A16) can be expressed as

$$f_\alpha = R_\alpha\left(a_{\alpha 1} w_\alpha + \frac{a_{\alpha 2}}{w_\alpha}\right) \tag{19}$$

where $a_{\alpha 1}$ and $a_{\alpha 2}$ are also constants to be determined by the boundary conditions. The boundary conditions along the unit circle, i.e. eqns (15)–(17) require

$$L_{ji}a_{i1}^* + \overline{L_{ji}a_{i2}^*} = 0, \quad j = 1,2,3 \quad \text{(traction-free)} \tag{20}$$

$$L_{4i}a_{i1}^* + \overline{L_{4i}a_{i2}^*} = -i\kappa^c(c - m\bar{c}) \quad \text{(surface charge-free)} \tag{21}$$

$$A_{4i}a_{i1}^* + \overline{A_{4i}a_{i2}^*} = c + m\bar{c} \quad \text{(irrotationality of electric fields).} \tag{22}$$

Solving eqns (20)–(22), the constants c and $\mathbf{a}_2^*$ can be expressed in terms of $\mathbf{a}_1^*$

$$c = i(\mathbf{B}_4 + \overline{\mathbf{B}_4})\frac{m(1+\kappa^c B_{44})\overline{\mathbf{L}\mathbf{a}_1^*} + (1-\kappa^c B_{44})\mathbf{L}\mathbf{a}_1^*}{m^2(1+\kappa^c B_{44})^2 - (1-\kappa^c B_{44})^2} \tag{23}$$

$$\mathbf{a}_2^* = \mathbf{L}^{-1}\bar{\mathbf{d}} - \mathbf{L}^{-1}\overline{\mathbf{L}\mathbf{a}_1^*} \tag{24}$$

where B_{44} is a negative real parameter in units of reciprocal dielectric constant (Lothe and Barnett, 1975; Suo *et al.*, 1992), and

$$\begin{aligned}
\mathbf{d} &= (0,0,0.d)^{\mathrm{T}} \\
d &= -i\kappa^c(c - m\bar{c}) \\
\mathbf{a}_1 &= (a_{11}, a_{21}, a_{31}, a_{41})^{\mathrm{T}} \\
\mathbf{a}_2 &= (a_{12}, a_{22}, a_{32}, a_{42})^{\mathrm{T}} \\
a_{i,1}^* &= \frac{R_i}{R}a_{i,1} \\
a_{i,2}^* &= \frac{R_i}{R}a_{i,2} \\
\mathbf{B}_4 &= (B_{41}, B_{42}, B_{43}, B_{44}).
\end{aligned} \tag{25}$$

The constant vector $\mathbf{a}_1$ can be determined from remote loading conditions. For a mode III crack in a piezoelectric material, there are four combinations of electric and mechanical loadings applied along the x_2-axis (Park, 1990; Zhang and Tong, 1996). For an infinite domain, in general, the remote electric loading is electric field strength E_i or electric displacement D_i, while the remote mechanical loadings are stresses σ_{ij} or strains ε_{ij}, as shown in Fig. 1. As they are connected by constitutive equations, only one of each counterpart pair is required to determine the constant vector $\mathbf{a}_1$. The remote extended stresses and strains are given by

$$\begin{aligned}
\lim_{z\to\infty} \Sigma_2 &= \mathbf{L}\mathbf{a}_1 + \overline{\mathbf{L}\mathbf{a}_1} = \Sigma_2^\infty \\
\lim_{z\to\infty} \Sigma_1 &= -\mathbf{L}\langle p_\alpha\rangle\mathbf{a}_1 - \bar{\mathbf{L}}\langle\overline{p_\alpha}\rangle\overline{\mathbf{a}_1} = \Sigma_1^\infty \\
\lim_{z\to\infty} \mathbf{S} &= \mathbf{C}^{-1}\lim_{z\to\infty}\Sigma = \mathbf{S}^\infty.
\end{aligned} \tag{26}$$

where the superscript "∞" refers to the remote applied extended loads, $\mathbf{S}$ is the extended

strain tensor, C is the extended elastic constant tensor, $\langle\ \rangle$ denotes a diagonal matrix, the superscript "-1" means reciprocal of a matrix, and

$$\Sigma_1 = (\sigma_{11}, \sigma_{21}, \sigma_{31}, D_1)^{\mathrm{T}}$$
$$\Sigma_2 = (\sigma_{12}, \sigma_{22}, \sigma_{32}, D_2)^{\mathrm{T}}. \tag{27}$$

From eqns (7), (18) and (23), the electric field inside the cavity can be obtained as

$$E^{\mathrm{c}} = -2c = -i2(\mathbf{B}_4 + \overline{\mathbf{B}_4})\frac{m(1+\kappa^{\mathrm{c}}B_{44})\overline{\mathbf{La}_1^*} + (1-\kappa^{\mathrm{c}}B_{44})\mathbf{La}_1^*}{m^2(1+\kappa^{\mathrm{c}}B_{44})^2 - (1-\kappa^{\mathrm{c}}B_{44})^2}. \tag{28}$$

Equation (28) indicates that the electric field within the cavity is uniform. This phenomenon was found in the previous work (Zhang and Tong, 1996). Defining the effective dielectric constant κ^{eff} as

$$\kappa^{\mathrm{eff}} = -1/B_{44} \tag{29}$$

and using the two dimensionless ratios α and β (Zhang and Tong, 1996)

$$\alpha = b/a$$
$$\beta = \kappa^{\mathrm{c}}/\kappa^{\mathrm{eff}} \tag{30}$$

we can rewrite eqn (28) as

$$E^{\mathrm{c}} = i(\mathbf{B}_4 + \overline{\mathbf{B}_4})\frac{(1-\alpha)(1-\beta)\overline{\mathbf{L}\langle 1 - ip_\alpha\alpha\rangle}\mathbf{a}_1 + (1+\alpha)(1+\beta)\mathbf{L}\langle 1 - ip_\alpha\alpha\rangle\mathbf{a}_1}{2(\alpha+\beta)(1+\alpha\beta)}. \tag{31}$$

From eqn (31), two extremes can be discussed. One is when the dielectric constant of the cavity is treated as zero, the electric field inside the cavity still has a finite value of

$$E^{\mathrm{c}} = i(\mathbf{B}_4 + \overline{\mathbf{B}_4})\frac{(1-\alpha)\overline{\mathbf{L}\langle 1 - ip_\alpha\alpha\rangle}\mathbf{a}_1 + (1+\alpha)\mathbf{L}\langle 1 - ip_\alpha\alpha\rangle\mathbf{a}_1}{2\alpha}. \tag{32}$$

Equation (32) shows that the electric field inside the cavity is influenced greatly by the dimensionless parameter α. The smaller α, the higher the electric field. The electric field approaches infinity as α approaches zero. Another extreme is the electric field inside the cavity nulls when the dielectric constant of the cavity approaches infinite, i.e. $\beta \to \infty$. The result is expected for a conducting crack. This behavior is similar to that for mode III cracks and more detailed discussions are given by Zhang and Tong (1996).

The extended displacements and stresses in the material are obtained as

$$\mathbf{u} = \mathbf{Af} + \overline{\mathbf{Af}} \tag{33}$$

$$\Sigma_2 = \mathbf{Lf}_{,1} + \overline{\mathbf{Lf}_{,1}}, \quad \Sigma_1 = -\mathbf{Lf}_{,2} - \overline{\mathbf{Lf}_{,2}} \tag{34}$$

where

$$f_\alpha = \frac{a_{\alpha 1}(z_\alpha + \sqrt{z_\alpha^2 - c_\alpha^2})}{2} + \frac{2R_\alpha^2 a_{\alpha 2}}{z_\alpha + \sqrt{z_\alpha^2 - c_\alpha^2}}$$
$$\mathbf{f}_{,1} = (f_{1,1}, f_{2,1}, f_{3,1}, f_{4,1})^{\mathrm{T}}, \quad \mathbf{f}_{,2} = (f_{1,2}, f_{2,2}, f_{3,2}, f_{4,2})^{\mathrm{T}}$$
$$f_{\alpha,1} = \left(a_{\alpha 1} - \frac{4R_\alpha^2 a_{\alpha 2}}{(z_\alpha + \sqrt{z_\alpha^2 - c_\alpha^2})^2}\right)\frac{z_\alpha + \sqrt{z_\alpha^2 - c_\alpha^2}}{2\sqrt{z_\alpha^2 - c_\alpha^2}}$$

$$f_{\alpha,2} = p_\alpha \left(a_{\alpha 1} - \frac{4R_\alpha^2 a_{\alpha 2}}{(z_\alpha + \sqrt{z_\alpha^2 - c_\alpha^2})^2} \right) \frac{z_\alpha + \sqrt{z_\alpha^2 - c_\alpha^2}}{2\sqrt{z_\alpha^2 - c_\alpha^2}}. \tag{35}$$

The extended strains can be calculated from the stress–strain correlation or from the extended displacements (see Appendix 1 for details).

3. ELECTRIC AND MECHANICAL FIELDS OF A SLIT CRACK

The electric field inside a crack can be obtained directly from eqn (31) by letting α approach zero. If the dielectric constant κ^c of the crack medium has a finite value (i.e. β is neither zero nor infinity), we have

$$E^c = i(\mathbf{B}_4 + \overline{\mathbf{B}_4}) \frac{(1-\beta)\overline{\mathbf{L}\mathbf{a}_1} + (1+\beta)\mathbf{L}\mathbf{a}_1}{2\beta}. \tag{36}$$

When β is much smaller than unity, eqn (36) shows that the electric field inside the crack is inversely proportional to β. As discussed before by Zhang and Tong (1996) for a mode III crack, the electric field inside a crack is related to the order of taking limits of α and β. Equation (31) shows that the electric field inside the crack will be zero if both β and $\alpha\beta$ approach infinity for an electrically conductive crack.

When the cavity reduces to a slit crack, the extended displacements and stresses have the same forms as given by eqns (33) and (34) with $f_\alpha, f_{\alpha,1}$ and $f_{\alpha,2}$ being reduced as

$$\begin{aligned} f_\alpha &= \frac{a_{\alpha 1}(z_\alpha + \sqrt{z_\alpha^2 - a^2})}{2} + \frac{a^2 a_{\alpha 2}}{z_\alpha + \sqrt{z_\alpha^2 - a^2}} \\ f_{\alpha,1} &= \left(a_{\alpha 1} - \frac{a^2 a_{\alpha 2}}{(z_\alpha + \sqrt{z_\alpha^2 - a^2})^2} \right) \frac{z_\alpha + \sqrt{z_\alpha^2 - a^2}}{2\sqrt{z_\alpha^2 - a^2}} \\ f_{\alpha,2} &= p_\alpha \left(a_{\alpha 1} - \frac{a^2 a_{\alpha 2}}{(z_\alpha + \sqrt{z_\alpha^2 - a^2})^2} \right) \frac{z_\alpha + \sqrt{z_\alpha^2 - a^2}}{2\sqrt{z_\alpha^2 - a^2}}. \end{aligned} \tag{37}$$

Define a complex stress intensity factor vector as

$$\mathbf{K}^* = \lim_{z_\alpha \to a} \mathbf{L} \langle \sqrt{2\pi(z_\alpha - a)} \rangle \mathbf{f}_1 \tag{38}$$

for the right crack tip. Substituting eqns (34) and (37) into eqn (38) and then completing the limiting process leads to

$$\mathbf{K}^* = \frac{\sqrt{\pi a}}{2} \mathbf{L}(\mathbf{a}_1 - \mathbf{a}_2) = \frac{\sqrt{\pi a}}{2} (\Sigma_2^\infty - \tilde{\mathbf{d}}). \tag{39}$$

Thus, the mode II, I and III intensity factors and the electric displacement intensity factor are twice the real part of the complex intensity factor vector

$$\begin{aligned} \mathbf{K} &= \mathbf{K}^* + \overline{\mathbf{K}^*} = \sqrt{\pi a}[\Sigma_2^\infty - (\mathbf{d} + \tilde{\mathbf{d}})] \\ \mathbf{K} &= (K_{\mathrm{II}}, K_{\mathrm{I}}, K_{\mathrm{III}}, K_{\mathrm{D}})^{\mathrm{T}}. \end{aligned} \tag{40}$$

Since the first three components in the $\mathbf{d}$ vector are zero, the first three components in the complex vector are real and correspondingly have the half values of the mode II, I and III stress intensity factors. However, the fourth component of the complex vector is, in general, a complex number and depends on the value of d. From eqns (23) and (25), we have

$$d = \left(\frac{\mathbf{B}_4 + \overline{\mathbf{B}_4}}{2B_{44}}\right)\frac{(1-\alpha^2)\overline{\mathbf{L}\langle 1 - ip_\alpha\alpha\rangle\mathbf{a}_1} + (1+\alpha^2+2\beta\alpha)\mathbf{L}\langle 1 - ip_\alpha\alpha\rangle\mathbf{a}_1}{(1+\alpha)[1+\alpha^2+\alpha/\beta+\alpha\beta]}. \tag{41}$$

The electric property of a crack can be divided into two classes: insulating and conducting. When $\alpha \to 0$, we have

$$d = \frac{(\mathbf{B}_4 + \overline{\mathbf{B}_4})\Sigma_2^\infty}{2B_{44}} \quad \text{for a finite } \beta \text{ or } \beta \to 0 \quad \text{and} \quad \alpha/\beta \to 0 \tag{42}$$

$$d = \frac{(\mathbf{B}_4 + \overline{\mathbf{B}_4})\Sigma_2^\infty}{2\mathbf{B}_{44}} \frac{1}{1+\dfrac{\alpha}{\beta}} \quad \text{for } \beta \to 0 \quad \text{and} \quad \alpha/\beta \text{ is finite} \tag{43}$$

$$d = 0 \quad \text{for } \beta \to 0 \quad \text{and} \quad \alpha/\beta \to \infty \tag{44}$$

for an insulating crack; and

$$d = \frac{(\mathbf{B}_4 + \overline{\mathbf{B}_4})\Sigma_2^\infty}{2B_{44}} \quad \text{for } \beta \to \infty \quad \text{and} \quad \alpha\beta \to 0 \tag{45}$$

$$d = \left[\frac{(\mathbf{B}_4 + \overline{\mathbf{B}_4})}{2B_{44}}\right]\frac{\Sigma_2^\infty + 2\mathbf{L}\mathbf{a}_1\alpha\beta}{1+\alpha\beta} \quad \text{for } \beta \to \infty \quad \text{and} \quad \alpha\beta \text{ is finite} \tag{46}$$

$$d = \frac{(\mathbf{B}_4 + \overline{\mathbf{B}_4})\mathbf{L}\mathbf{a}_1}{B_{44}} \quad \text{for } \beta \to \infty \quad \text{and} \quad \alpha\beta \to \infty \tag{47}$$

for a conducting crack. It can be seen in eqn (44) that $d = 0$ is appropriate only when $\beta \to 0$ and $\alpha/\beta \to \infty$. In this case, the electric displacement intensity factor has the conventional form: $K_D = \sqrt{\pi a} D_2^\infty$ (Suo *et al.*, 1992). For most PZT ceramics containing a vacuum flaw with the smallest dielectric constant, the ratio of the dielectric constant of the crack to the effective dielectric constant of the material is at the order of 10^{-3}. To satisfy the conditions for $d = 0$ requires that $\alpha = b/a \geqslant 0.01$. Caution must be used here to employ the fracture mechanics to treat a real cavity and this situation has been discussed in previous work (Zhang, 1994a). It can be seen in eqns (42)–(44) that the parameter d is real. In this case, the extended displacements and stresses in the vicinity of the crack tip can be expressed in terms of the mode II, I, III intensity factors and the electric displacement intensity factor and the complex intensity factors are not needed here. It should be noted that the conventional definition for the electric displacement intensity factor fails for the insulating crack if d does not equal zero. Equations (45)–(47) show that d is not zero for a conducting crack. Under conditions that $\beta \to \infty$ and $\alpha\beta \to 0$, d is real for a conducting crack. However, under conditions that $\beta \to \infty$ and $\alpha\beta$ is finite, and $\beta \to \infty$ and $\alpha\beta \to \infty$, d has, in general, a complex value because $\mathbf{L}\mathbf{a}_1$ is primarily a complex parameter which depends on the material properties, the crack orientation and the remote loadings. Thus, the four conventional intensity factors are not sufficient to describe the mechanical and electric fields in the vicinity of a conducting crack tip for the linear anisotropic piezoelectric materials under combined mechanical–electrical loadings. In this case, a general complex vector of intensity factors is necessary for this analysis.

When the origin of the system is moved to the right crack tip, we introduced new variables $z_\alpha^* = z_\alpha - a$. Then, the electric and mechanical fields near the right crack tip can be expressed in terms of the complex stress intensity factors as

$$\Sigma_2 = \mathbf{L}\left\langle \frac{1}{\sqrt{2\pi z_\alpha^*}} \right\rangle \mathbf{L}^{-1}\mathbf{K}^* + \bar{\mathbf{L}}\left\langle \frac{1}{\sqrt{2\pi \bar{z}_\alpha^*}} \right\rangle \overline{\mathbf{L}^{-1}\mathbf{K}^*}$$

$$\Sigma_1 = -\mathbf{L}\left\langle \frac{p_\alpha}{\sqrt{2\pi z_\alpha^*}} \right\rangle \mathbf{L}^{-1}\mathbf{K}^* - \bar{\mathbf{L}}\left\langle \frac{\bar{p}_\alpha}{\sqrt{2\pi \bar{z}_\alpha^*}} \right\rangle \overline{\mathbf{L}^{-1}\mathbf{K}^*}. \tag{48}$$

The crack tip extended opening is calculated by

$$\Delta\mathbf{u} = \mathbf{u}^+ - \mathbf{u}^- \tag{49}$$

where the superscript "+" and "−" denote, respectively, the "upper" and "lower" crack faces. Substituting eqn (33) into eqn (49) yields the extended crack opening as

$$\Delta\mathbf{u} = a(i(\mathbf{A}\mathbf{a}_1 - \overline{\mathbf{A}\mathbf{a}_1}) - i(\mathbf{A}\mathbf{a}_2 - \overline{\mathbf{A}\mathbf{a}_2}))\sin\theta, \quad 0 \leqslant \theta \leqslant \pi. \tag{50}$$

Equation (50) shows that the crack opening has an elliptical profile. Near the crack tip, the extended displacements can be expressed in teams of the complex vector of the intensity factors as

$$\mathbf{u} = \mathbf{A}\left\langle \frac{\sqrt{2z_\alpha^*}}{\sqrt{\pi}} \right\rangle \mathbf{L}^{-1}\mathbf{K}^* + \bar{\mathbf{A}}\left\langle \frac{\sqrt{2\bar{z}_\alpha^*}}{\sqrt{\pi}} \right\rangle \overline{\mathbf{L}^{-1}\mathbf{K}^*}. \tag{51}$$

Similarly, the extended crack opening near the crack tip is given by:

$$\Delta\mathbf{u} = \frac{2\sqrt{2r}}{\sqrt{\pi}}[\mathbf{B}\mathbf{K}^* + \overline{\mathbf{B}\mathbf{K}^*}] \tag{52}$$

where r is the distance from the crack tip.

4. THE ENERGY RELEASE RATE FOR CRACK OR CAVITY PROPAGATION

The energy release rate can be evaluated from each of the four thermodynamic functions: free energy, electric enthalpy, mechanical enthalpy and full Gibbs energy, or from each of the four associate potentials. Details are described in Appendix 2. In the present work, we follow Rice's treatment (1968) and use the potential associated with the electric enthalpy to formulate the energy release rate. Using the same principle and methodology, we first derive the energy release rate for an elliptical cavity, as shown in Fig. 1, under the condition that the ratio of the minor semi-axis to the major semi-axis, $\alpha = b/a$ is maintained unchanged. When the elliptical cavity reduces to a slit crack, the energy release rate will automatically respond for slit crack propagation. Since only two-dimensional problems are treated here, all properties are calculated per thickness. In this case, the crack area $A = 1 \times a = a$. Thus, the energy release rate is given by

$$2J = \frac{\partial P_{\mathrm{H}}}{\partial a} = \int_\Gamma \left(t_i \frac{\partial u_i}{\partial a} + D_i \frac{\partial \phi n_i}{\partial a} \right) \mathrm{d}\Gamma - \frac{\partial}{\partial a}\int_\Pi h\,\mathrm{d}\Pi. \tag{53}$$

A factor of two is added here due to two crack tips in this system. Using the solutions given in previous section and after tedious algebraic calculation, finally, we have

$$J = \frac{\pi a}{4}[(\Sigma_2^\infty)^{\mathrm{T}}(\mathbf{B}+\bar{\mathbf{B}})\Sigma_2^\infty - (1+\alpha)(\Sigma_2^\infty)^{\mathrm{T}}(\mathbf{B}\bar{\mathbf{d}} + \bar{\mathbf{B}}\mathbf{d})$$

$$+\alpha^2(\Sigma_1^\infty)^{\mathrm{T}}(\mathbf{B}+\bar{\mathbf{B}})\Sigma_1^\infty - i\alpha(1+\alpha)(\Sigma_1^\infty)^{\mathrm{T}}(\mathbf{B}\bar{\mathbf{d}} - \bar{\mathbf{B}}\mathbf{d})$$

$$-[i(1+\alpha)(\bar{\mathbf{d}}-\mathbf{d})-2\alpha\Sigma_1^{\infty}]^{\mathrm{T}}(\mathbf{A}\mathbf{a}_1+\overline{\mathbf{A}\mathbf{a}_1})$$
$$-\alpha[(1+\alpha)(\bar{\mathbf{d}}+\mathbf{d})-2\Sigma_2^{\infty}]^{\mathrm{T}}[\mathbf{A}\langle p_\alpha\rangle\mathbf{a}_1+\bar{\mathbf{A}}\langle\overline{p_\alpha}\rangle\overline{\mathbf{a}_1}]]. \tag{54}$$

Equation (54) shows that the energy release rate for an elliptical cavity growth depends on both mechanical and electric loads, as well as the ratio of $\alpha = b/a$ and the value of the dielectric constant κ^c inside the cavity.

When the cavity reduces to a slit crack (i.e. $\alpha = b/a = 0$) and the dielectric constant of the crack medium κ^c has a finite value (for example, $\kappa^c = 8.85 \times 10^{-12}$ F/m for a vacuum crack), d is real and the energy release rate for the crack propagation is reduced to

$$J = \frac{\pi a}{4}[(\Sigma_2^{\infty})^{\mathrm{T}}(\mathbf{B}+\bar{\mathbf{B}})(\Sigma_2^{\infty}-\mathbf{d})]. \tag{55}$$

If the crack is an electrically conductive crack with κ^c being infinite, the energy release rate is

$$J = \frac{\pi a}{4}[(\Sigma_2^{\infty})^{\mathrm{T}}(\mathbf{B}+\bar{\mathbf{B}})\Sigma_2^{\infty}-(\Sigma_2^{\infty})^{\mathrm{T}}(\mathbf{B}\bar{\mathbf{d}}+\bar{\mathbf{B}}\mathbf{d})-i(\bar{\mathbf{d}}-\mathbf{d})^{\mathrm{T}}(\mathbf{A}\mathbf{a}_1+\overline{\mathbf{A}\mathbf{a}_1})]. \tag{56}$$

If the parameter $d = 0$, however, the energy release rate for the crack propagation is

$$J = \frac{\pi a}{4}(\Sigma_2^{\infty})^{\mathrm{T}}(\mathbf{B}+\bar{\mathbf{B}})\Sigma_2^{\infty}. \tag{57}$$

Equation (57) is the conventional result from the electric boundary condition that the electric displacement component perpendicular to the crack faces is zero along the crack faces. Equations (55), (56) and (57) will be compared explicitly in Section 6 regarding the contribution of applied electric loadings.

5. SELF-CONSISTENT CALCULATION OF CRACK PROFILE

Under a pure mechanical loading for small deformation, conventional linear elastic fracture analysis uses the crack profile before deformation to evaluate the stress fields and the energy release rate. In previous sections we also employed this approach and systematically formulated the stress and displacement fields as well as the energy release rate for coupled mechanical and electric problems. However, it is noted that under combined mechanical and electric loadings, the crack opens and the crack deformation is very sensitive to the electric field (inside the opened crack) which in turn, is affected by the opened crack profile. So a geometrically nonlinear electro-elastic analysis, here called self-consistent calculation, is adopted to determine the deformed crack profile and subsequently the energy release rate for the crack propagation.

For a slit crack, the crack opening along the x_2 axis, Δu_2 from conventional calculations is given by eqn (50) which can be further arranged as

$$\Delta u_2 = a[(\mathbf{B}+\bar{\mathbf{B}})(\Sigma_2^a-\mathbf{d})]_2 \sin\theta, \quad 0 \leqslant \theta \leqslant \pi. \tag{58}$$

Clearly, the profile of crack opening is an ellipse with the major semi-axis of a and the minor semi-axis of $b = a/2[(\mathbf{B}+\bar{\mathbf{B}})(\Sigma_2^a-\mathbf{d})]_2$, where subscript 2 means the second term in the vector. Thus, the ratio α_c of the minor semi-axis to the major semi-axis evaluated from the conventional calculation is:

$$\alpha_c = \tfrac{1}{2}[(\mathbf{B}+\bar{\mathbf{B}})(\Sigma_2^a - \mathbf{d})]_2 \tag{59}$$

which will be compared with the results obtained from the self-consistent calculation later.

The self-consistent method requires that the half maximum opening of the elliptical cylinder cavity should be equal to the minor semi-axis. That means

$$\alpha_s = [\mathbf{A}\mathbf{f}(\alpha_s) + \overline{\mathbf{A}\mathbf{f}(\alpha_s)}]_2 \quad \text{at } (0,0) \tag{60}$$

where α_s is the ratio of the minor semi-axis to the major semi-axis in the self-consistent calculation and $\mathbf{f}(\alpha_s)$ is a four-dimensional vector and a function of α_s and the remote loadings. After tedious algebraic calculation, eqn (60) is finally re-arranged as

$$g_0 + g_1\alpha_s + g_2\alpha_s^2 + g_3\alpha_s^3 = 0 \tag{61}$$

where

$$\begin{aligned}
g_0 &= \kappa^c B_{44}[(\mathbf{B}+\bar{\mathbf{B}})\Sigma_2^a]_2 - \frac{\kappa^c}{2}(B_{24}+\overline{B_{24}})(B_{4k}+\overline{B_{4k}})\Sigma_2^a \\
g_1 &= \kappa^c B_{44}C_0 - (1+\kappa^c B_{44}^2\kappa^c)[(\mathbf{B}+\bar{\mathbf{B}})\Sigma_2^a]_2 - \frac{\kappa^c}{2}(B_{4k}+\overline{B_{4k}})C_1 \\
g_2 &= \kappa^c B_{44}[(\mathbf{B}+\bar{\mathbf{B}})\Sigma_2^a]_2 - (1+\kappa^c B_{44}^2\kappa^c)C_0 \\
&\quad - \frac{\kappa^c}{2}(B_{24}+\overline{B_{24}})(B_{4k}+\overline{B_{4k}})\Sigma_2^a - \kappa^c(B_{4k}+\overline{B_{4k}})C_2 \\
g_3 &= \kappa^c B_{44}C_0 - i\frac{\kappa^c}{2}(\overline{B_{24}}-B_{24})(B_{4k}+\overline{B_{4k}})\Sigma_1^a \\
C_0 &= [i(\bar{\mathbf{B}}-\mathbf{B})\Sigma_1^a + 2(\mathbf{A}\langle\mathbf{p}_\alpha\rangle\mathbf{a}_1 + \bar{\mathbf{A}}\langle\overline{\mathbf{p}_\alpha}\rangle\overline{\mathbf{a}_1})]_2 - 2 \\
C_1 &= -2\kappa^c B_{44}(\mathbf{B}_{24}\overline{\mathbf{L}\mathbf{a}_1} + \overline{\mathbf{B}_{24}}\mathbf{L}\mathbf{a}_1) - i(B_{24}+\overline{B_{24}})[\mathbf{L}\langle\mathbf{p}\rangle\mathbf{a}_1 - \bar{\mathbf{L}}\langle\bar{\mathbf{p}}\rangle\overline{\mathbf{a}_1}] \\
C_2 &= (\mathbf{B}_{24}\mathbf{L}\mathbf{a}_1 + \overline{\mathbf{B}_{24}\mathbf{L}\mathbf{a}_1}) + i\kappa^c B_{44}(\overline{\mathbf{B}_{24}}\mathbf{L}\langle\mathbf{p}\rangle\mathbf{a}_1 - \mathbf{B}_{24}\bar{\mathbf{L}}\langle\bar{\mathbf{p}}\rangle\overline{\mathbf{a}_1}).
\end{aligned} \tag{62}$$

After careful checking of eqn (62), we found that these four parameters, g_0, g_1, g_2 and g_3 are all real. Thus, the real root to eqn (61) is given by

$$\alpha_s = \left[-\frac{g_0^*}{2} + \sqrt{\left(\frac{g_0^*}{2}\right)^2 + \left(\frac{g_1^*}{3}\right)^3}\right]^{1/3} + \left[-\frac{g_0^*}{2} - \sqrt{\left(\frac{g_0^*}{2}\right)^2 + \left(\frac{g_1^*}{3}\right)^3}\right]^{1/3} - \frac{g_2}{3g_3} \tag{63}$$

where

$$\begin{aligned}
g_0^* &= \frac{g_0}{g_3} - \frac{g_1 g_2}{3g_3^2} + 2\left(\frac{g_2}{3g_3}\right)^3 \\
g_1^* &= \frac{g_1}{g_3} - 3\left(\frac{g_2}{3g_3}\right)^2.
\end{aligned} \tag{64}$$

In the next section, the crack opening will be numerically calculated and plotted.

6. RESULTS AND DISCUSSION

In this section, we numerically calculate and plot the results under different loading conditions. For simplicity, hereafter, we ignore the superscript "E" for the elastic constants

and the superscript "e" for the dielectric constants. If the x_2 direction is parallel to the poling direction, the constitutive relation is given by

$$\begin{bmatrix} \sigma_{11} \\ \sigma_{22} \\ \sigma_{33} \\ \sigma_{23} \\ \sigma_{13} \\ \sigma_{12} \\ D_1 \\ D_2 \\ D_3 \end{bmatrix} = \begin{bmatrix} c_{11} & c_{13} & c_{12} & 0 & 0 & 0 & 0 & e_{31} & 0 \\ c_{13} & c_{33} & c_{13} & 0 & 0 & 0 & 0 & e_{33} & 0 \\ c_{12} & c_{13} & c_{11} & 0 & 0 & 0 & 0 & e_{31} & 0 \\ 0 & 0 & 0 & c_{44} & 0 & 0 & 0 & 0 & e_{15} \\ 0 & 0 & 0 & 0 & (c_{11}-c_{12})/2 & 0 & 0 & 0 & 0 \\ 0 & 0 & 0 & 0 & 0 & c_{44} & e_{15} & 0 & 0 \\ 0 & 0 & 0 & 0 & 0 & e_{15} & -\kappa_{11} & 0 & 0 \\ e_{31} & e_{33} & e_{31} & 0 & 0 & 0 & 0 & -\kappa_{33} & 0 \\ 0 & 0 & 0 & e_{15} & 0 & 0 & 0 & 0 & -\kappa_{11} \end{bmatrix} \begin{bmatrix} \varepsilon_{11} \\ \varepsilon_{22} \\ \varepsilon_{33} \\ 2\varepsilon_{23} \\ 2\varepsilon_{13} \\ 2\varepsilon_{12} \\ -E_1 \\ -E_2 \\ -E_3 \end{bmatrix}. \tag{65}$$

The **N** matrix is formulated in Appendix 3 for this orientation. Then, the eigen-equation, i.e. eqn (A18) is solved using the commercial code, MATLAB.

The present work uses the PZT-4 ceramics as a model material. The material constants are given below:

Elastic constants (10^{10} N/m^2):

$$c_{11} = 13.9, \quad c_{12} = 7.78, \quad c_{13} = 7.43, \quad c_{33} = 11.3, \quad c_{44} = 2.56;$$

Piezoelectric constants (C/m^2):

$$e_{31} = -6.98, \quad e_{33} = 13.84, \quad e_{15} = 13.44;$$

Dielectric constants (10^{-9} F/m):

$$\kappa_{11} = 6.00, \quad \kappa_{33} = 5.47; \quad \kappa^e = 8.85 \times 10^{-3}; \tag{66}$$

where N and C denote, respectively Newton's and Coulombs. The dielectric constant of vacuum, κ^e, is listed here again for convenience.

In order to verify the validity of the formulas derived in previous sections, we resort to the finite element analysis and the commercial software ABAQUS is used. The example considered is a finite medium with a centered crack or elliptical cavity under both mechanical and electrical loadings. The specimen dimensions, finite element mesh and loading conditions are shown in Fig. 3(a) for the case of a centered elliptical cavity with Fig. 3(b) being the magnification of the mesh around the cavity. As the medium size is much larger than that of the crack or cavity, the near tip solution should be nearly the same as that for the infinite medium. Eight-noded plane strain elements were used in the analysis.

Figure 4 shows the distribution of the stress σ_{22} and electric field E_2 in front of the right major axial apex of an elliptical cavity with the major semi-axis $a = 1$ m and the minor semi-axis $b = 0.2$ m under combined mechanical and electrical loadings in the x_2-direction. The other mechanical and electric loadings not specified in the figure are zero and this convention will apply for all figures in the following discussion. As expected, both the stress and the electric field are concentrated at the apex of the cavity, as shown in Fig. 4. The stress and electric concentrations increase as the parameter α decreases. When α approaches zero, the cavity reduces to a slit crack. Figure 5 shows the distribution of the stress σ_{22} and electric field E_{22} in the crack line for a slit crack. Like the case of a pure Mode III crack (Zhang and Tong, 1996), the mechanical stresses and electric fields at the crack tip have totally different behaviors. The stresses are singular at the crack tip, but the electric fields are not and the boundary condition by eqn (22) requires that E_2 in the material must

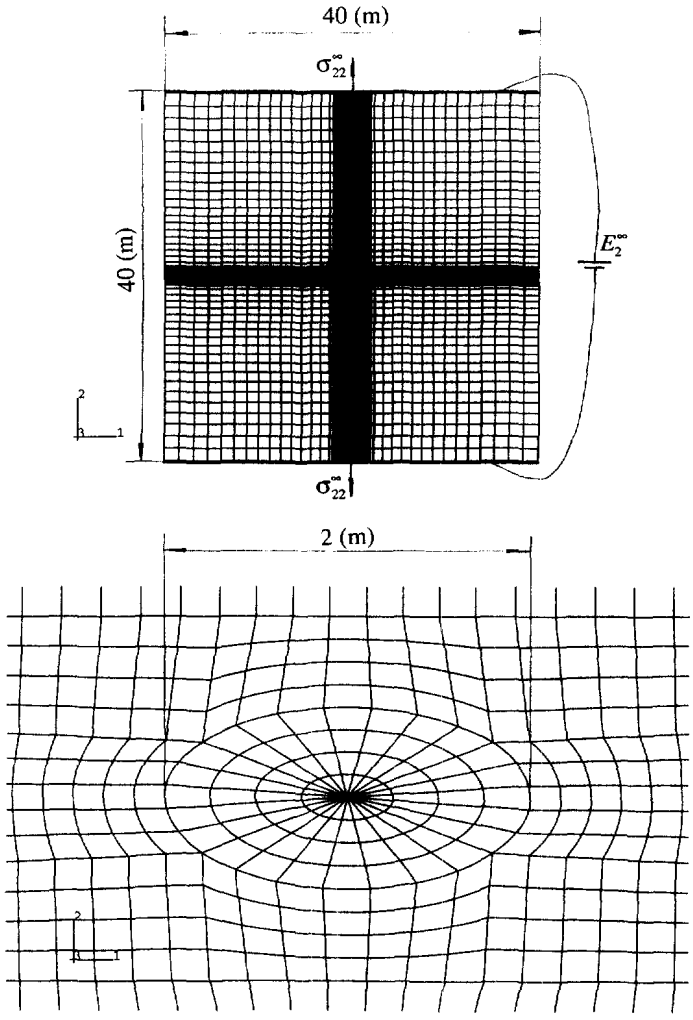

Fig. 3. (a) Finite element mesh for a centered elliptical cavity in a large piezoelectric medium under combined mechanical–electrical loadings; (b) fine mesh around the cavity.

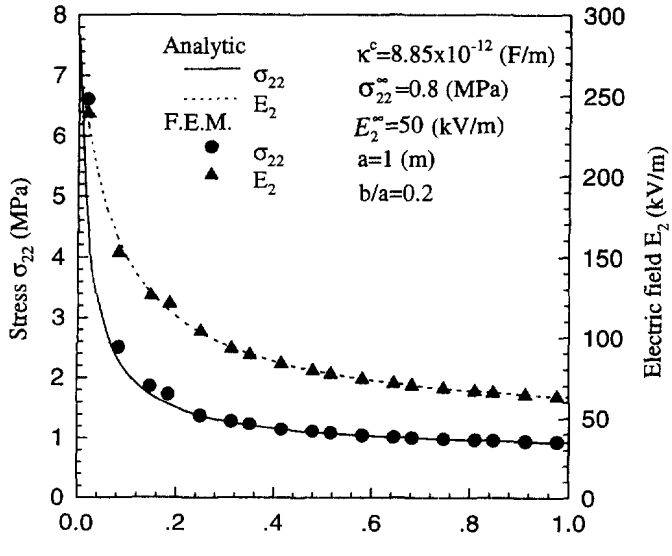

Fig. 4. Distribution of stress σ_{22} and electric field E_2 ahead of an elliptical cavity.

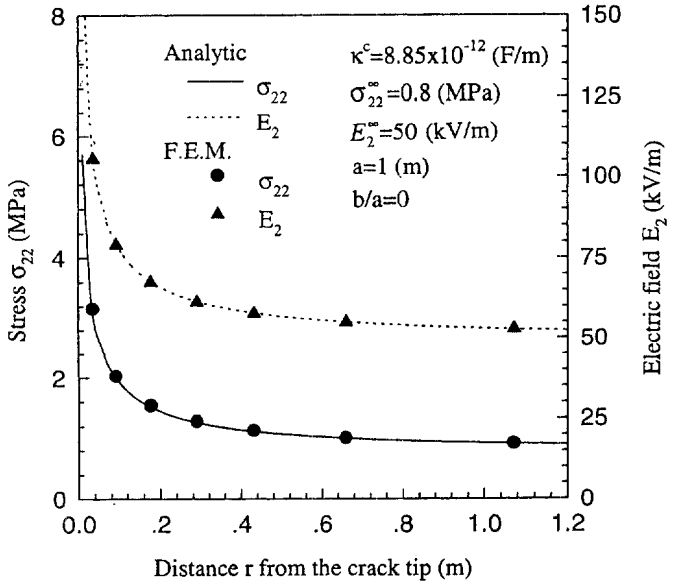

Fig. 5. Distribution of stress σ_{22} and electric field E_2 ahead of a crack tip.

be equal to that in the crack. From eqns (33) and (37), it can be derived that E_2 at the crack tip in the material is

$$E_2 = 1133.72E_2^{\infty} - 20.16\sigma_{11}^{\infty} - 1.53\sigma_{22}^{\infty} \tag{67}$$

where E_2 and E_2^{∞} and σ_{11}^{∞} and σ_{22}^{∞} are, respectively, in units of V/m and Pa.

Figures 4 and 5 show that the analytical results agree well with the finite element analysis, which indicates that the analytical solutions formulated in Sections 2 and 3 are valid for both an elliptical cylinder cavity and a slit crack.

When the cavity is reduced to a slit crack and the crack medium is considered as a vacuum, the electric field inside the crack and the energy release rate for the crack propagation under in-plane combined mechanical–electrical loadings can be further simplified explicitly as

$$\begin{aligned} E_1 &= E_1^{\infty} + 0.0188\sigma_{12}^{\infty} \\ E_2 &= 1133.72E_2^{\infty} - 20.16\sigma_{11}^{\infty} - 1.53\sigma_{22}^{\infty} \\ J &= [2.77(\sigma_{12}^{\infty})^2 + 3.63(\sigma_{22}^{\infty})^2]a \times 10^{-11} \end{aligned} \tag{68}$$

where a, E_i, σ_{ij} and J are, respectively, in units of m, V/m, Pa and N/m and hereafter the same units are used for those properties, and high-order small terms are ignored in eqn (68). The expression for E_2 in the crack by eqn (68) is exactly the same as that for E_2 at the crack tip in the material, as shown by eqn (67), which is a direct consequence of the continuity of the tangential component of the electric field strength. It is seen from eqn (68) that the component of electric field strength E_2 inside the crack is more than 1000 times greater than the applied electric field, while the energy release rate J is independent of either the applied electric fields or the mechanical loading parallel to the crack surface, i.e. σ_{11}^{∞}.

When the parameter d is considered zero, the energy release rate for the crack propagation by eqn (57) can be expressed explicitly as

$$\begin{aligned} J = [&4.37 \times 10^{-3}(\sigma_{11}^{\infty})^2 + 2.77 \times 10^{-2}(\sigma_{12}^{\infty})^2 + 3.63 \times 10^{-2}(\sigma_{22}^{\infty})^2 \\ &+ 0.492\sigma_{11}^{\infty}E_2^{\infty} + 3.73 \times 10^{-2}\sigma_{22}^{\infty}E_2^{\infty} - 13.83(E_2^{\infty})^2]a \times 10^{-9} \end{aligned} \tag{69}$$

which has almost the same form as the results obtained by Park and Sun (1995) in the

absence of σ_{11}^{∞} and σ_{12}^{∞}. In this case, the energy release rate decreases with increasing the applied electric field E_2^{∞}, implying that the applied electric loading will impede the crack propagation.

Finite element evaluation of the energy release rate J is based on (Cherepanov, 1979)

$$J = \int_{\Gamma} (hn_1 - \sigma_{ij} n_j u_{i,1} + D_i E_1 n_i)\, \mathrm{d}\Gamma, \quad i,j,k = 1,2,3 \tag{70}$$

where $h = 1/2 c_{ikl}\varepsilon_{ij}\varepsilon_{kl} - 1/2\kappa_{ij}E_iE_j - e_{ijkl}\varepsilon_{kl}E_i$ is the electric enthalpy per unit volume; Γ is an integration contour around the crack tip or ellipse apex, $\mathbf{n}$ is the unit normal vector to the contour. When the crack faces are free of external charge and traction, J is path independent (Cherepanov, 1979; Suo *et al.*, 1992).

Figure 6 shows the electric field at the crack tip and the energy release rate calculated from eqns (68) and (69) together with the results from the finite element analysis. Again, the theoretical prediction agrees with the finite element calculation. With all relevant formulas being verified by finite element analysis, hereafter, we will no longer present the finite element results in the following discussion. As can be seen in Fig. 6, the energy release rate is independent of the applied electric field when the electric field inside the slit crack is taken into account. A mathematical slit crack does not have any width and the perpendicular component of the displacement continues cross the crack faces. Consequently, the electrical field far ahead of the crack tip is equivalent to that far behind the crack tip. Therefore, the applied electric field does not contribute to the energy release rate (Zhang, 1994a). If the electric field inside the crack is ignored, i.e. $\kappa^c = 0$, however, the applied electric field impedes crack propagation (Suo *et al.*, 1992).

As described in both Section 4 and Appendix 2, the energy release rate can be calculated from the four potentials. Since the mechanical displacement and the electric potential are chosen as independent variables, it is convenient to use the electric enthalpy and its associate potential to evaluate the energy release rate for the elliptical cavity. An ellipse has two parameters, the minor semi-axis b and the major semi-axis a. When the cavity changes its size while maintains its shape, the potential associate with the electric enthalpy changes. The energy release rate for the cavity is defined in the present study as a ratio of infinitesimal change in the potential over infinitesimal change in the cavity size, while the cavity shape remains unchanged. For a given cavity, both the electric field inside the cavity and the energy release rate are functions of the remote mechanical and electrical loadings, as shown

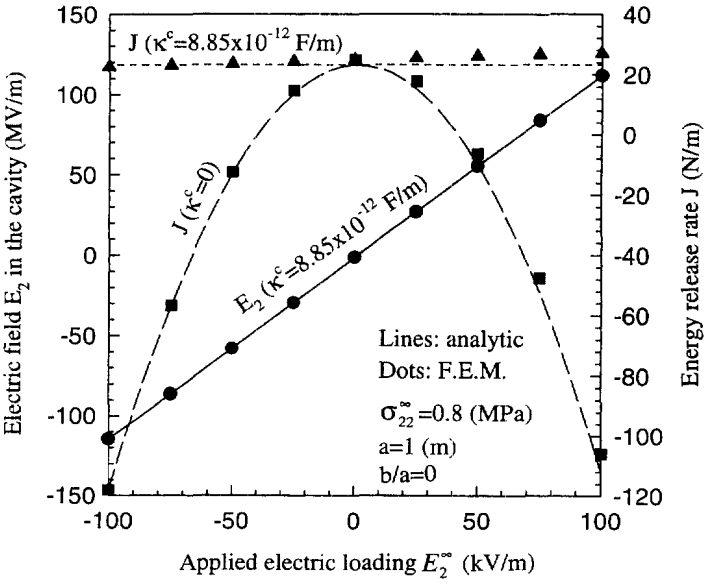

Fig. 6. Electric field and energy release rate as a function of applied electric loading for a slit crack.

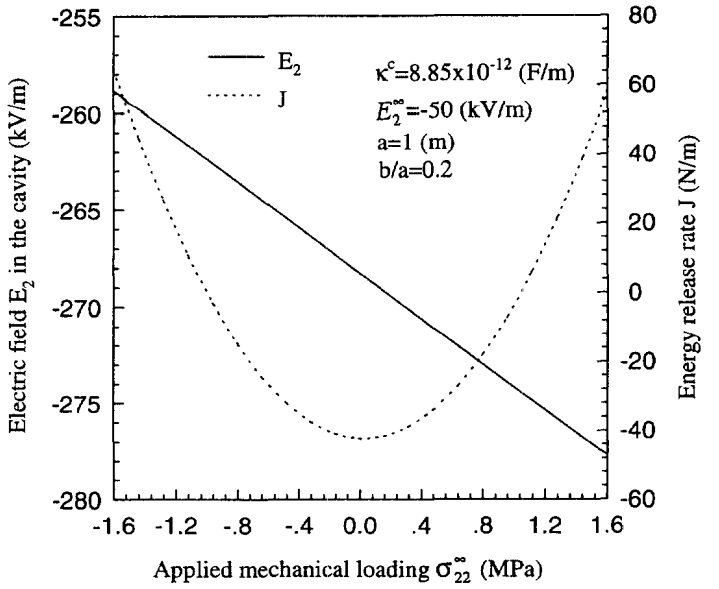

Fig. 7. Electric field and energy release rate as a function of applied mechanical loading for a vacuum cavity.

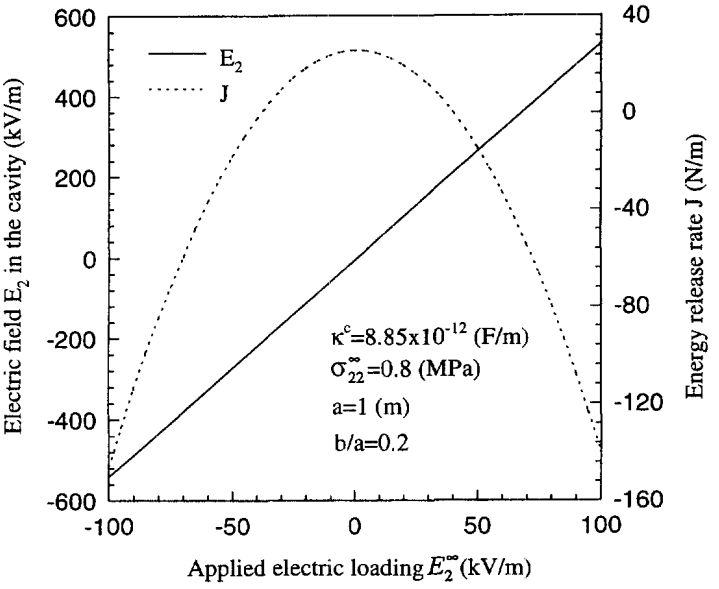

Fig. 8. Electric field and energy release rate as a function of applied electric loading for a vacuum cavity.

in eqns (28) and (54). We plot eqns (28) and (54) in Figs 7 and 8 to illustrate the relationships.

Figure 7 shows the variations of the electric field inside the cavity and the energy release rate with the applied stress under a constant applied electric field. The electric field inside the cavity is about five times greater than that of the applied electric field and increases its absolute magnitude with increasing applied stress. The energy release rate increases also when the absolute value of the applied stress increases. It should be noted that for an elliptical cavity the energy release rate increases with increasing absolute value of a compressive-applied stress as long as the upper and lower faces of the cavity do not contact one another. When the upper and lower faces of the cavity come into contact, which could be the case for a slit crack under compression, the traction-free condition along the cavity faces no longer holds and the energy release rate loses its meaning. Figure 8 indicates the electric field inside the cavity and the energy release rate as functions of the

applied electric field under a constant applied stress. The electric field strength inside the cavity is directly proportional to the applied electric field with a slope about five. Since the cavity has a finite width, either a positive or a negative applied electric field decreases the energy release rate, as shown in Fig. 8. This result indicates that the influence of the applied electric field on the energy release rate depends on the shape of the cavity. An insulating crack opens under applied mechanical loads, the applied electric field will then contribute itself to the energy release rate if the opened crack profile is considered. We will discuss this case later.

To demonstrate the influence of the electric property of the cavity medium, we consider another extreme, a conducting cavity having an infinitely large dielectric constant. In this case, the electric field inside the cavity is zero. Figure 9 shows the energy release rate J for the cavity propagation as a function of the applied electric loading E_1^∞ or E_2^∞ without applying any mechanical load. The energy release rate J is positive definite with respect to the applied electric loadings. An electrically-positive-definite energy release rate means that the electrical loading would propagate the crack rather than impede it. Comparing Figs 9 and 8 indicates that the electric behavior for the conducting cavity differs totally from that for the vacuum cavity. As can be seen in Fig. 9, E_1^∞ makes a greater contribution to the energy release rate than E_2^∞, when the two being at the same level of magnitude. It is E_1^∞ rather than E_2^∞ that causes the electrostrictive effect to the cavity and, consequently, promotes the cavity propagation. For the conducting cavity, the energy release rate J is also positive definite with respect to the applied mechanical loading, as shown in Fig. 10. Thus, the energy release rate for a conducting crack is always positive definite under the combined mechanical–electrical loadings. For a vacuum cavity, however, the energy release rate J could be negative when the electrical loading is high and the mechanical loading is low (see Fig. 7). Figure 10 shows that with the same level of magnitude, σ_{12}^∞ makes the largest contribution to the energy release rate among the three loading modes. In particular σ_{11}^∞ can also propagate the crack due to the anisotropic and piezoelectric properties of the poled ceramics.

For an electrically conductive crack, the energy release rate J formulated by eqn (56) can be explicitly represented with sufficient accuracy as

$$J = [17.96(E_1^\infty)^2 + 3.403 \times 10^{-2}(\sigma_{12}^\infty)^2 + 3.63 \times 10^{-2}(\sigma_{22}^\infty)^2]a \times 10^{-9}. \tag{71}$$

When the cavity is reduced to a slit crack, eqn (71) shows that the applied electric field

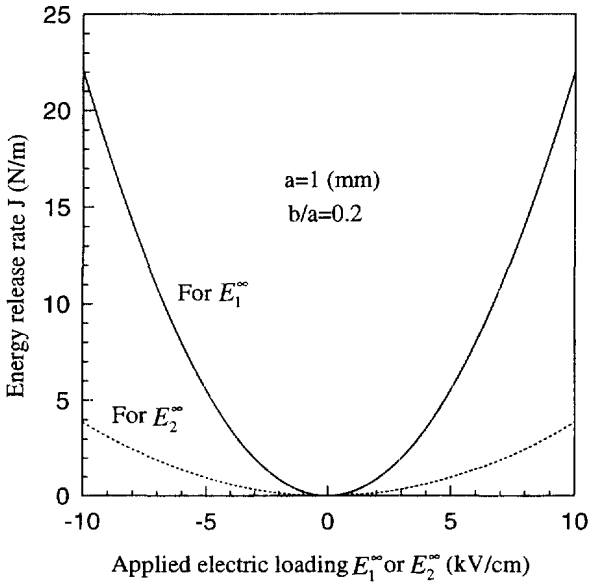

Fig. 9. Energy release rate as a function of applied electric loading for an electrically conductive cavity.

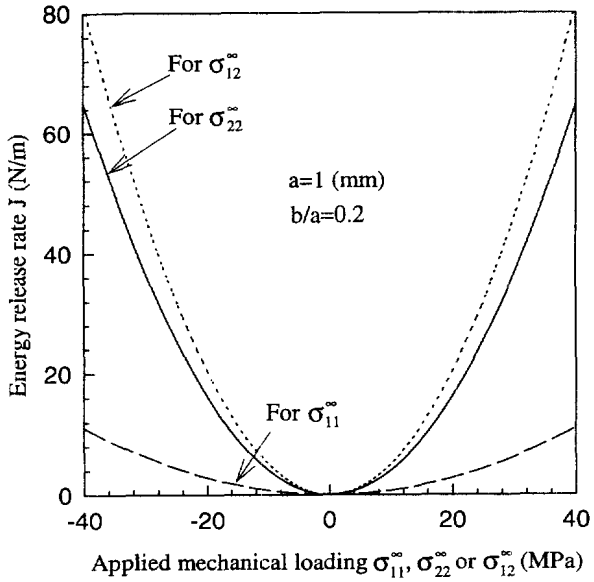

Fig. 10. Energy release rate as a function of applied mechanical loading for an electrically conductive cavity.

perpendicular to the crack, i.e. E_2^{∞}, does not contribute anything to the energy release rate, because a conductive crack does not change the electric field along the x_2-axis, i.e. E_2, in both regions far ahead and far behind the crack tip. Equation (71) indicates that the energy release rate J for a conductive crack is quadratic function of the applied mechanical loadings and the applied electric field along the x_1-axis, i.e. the electric field parallel to the conductive crack. The finding that an electric loading parallel to the crack can propagate a conducting crack are qualitatively consistent with McMeeking's (1987) results for isotropic dielectric ceramics. As discussed above, the contribution from E_1^{∞} is mainly due to the electrostrictive effect and this effect is much more significant for a conducting crack than a conducting cavity. It is clear that different electric properties (i.e. different dielectric constants) of slit cracks lead to totally different results regarding the contribution of applied electric loadings to crack propagation.

We have studied also the case that the poling direction is parallel to the x_1-axis, and the results are similar to those described above for the poling direction parallel to the x_2-axis. Therefore, those results are not repeated again in the present study.

As discussed above, the energy release rate J for a slit crack with dielectric constant $\kappa^c = 8.85 \times 10^{-12}$ (F/m) is independent of applied electric loadings in the linear analysis using the undeformed crack profile. Under the applied tensile loading the crack opens and the deformed crack surface profile constitutes an ellipse form as shown in eqn (58) for the opening of the crack faces, although the ellipse will be very "flat". As soon as the crack opens and becomes an elliptical cavity, the effects of applied electric loadings on the energy release rate emerges, as shown in Fig. 8. In order to study the effects of the applied electric field on the energy release rate we have to consider the crack opening. In principal, the applied electric field could influence also the crack opening. Thus, it is more reasonable to determine the final crack surface profile under combined mechanical and electric loadings by introducing an elliptical crack geometry with a to-be-determined minor semi-axis. Figure 11 shows α_s evaluated from the self-consistent calculation by eqn (60), together with α_c for a list crack obtained from conventional calculation by eqn (59) as a function of the electric loading E_2^{∞}. It is found that if the electric loading is zero, α_s is equal to α_c and both are proportional to the mechanical loading σ_{22}^{∞}. If the electric loading is not zero, however, α_s is different from α_c and the difference becomes larger as the magnitude of the electric field increases. It is also found from Fig. 11 that the direction of the electric loading also affects the value of α_s (i.e. the opening of the crack). Compared with the crack opening without electric loadings, a positive applied electric loading makes the crack opening larger while a negative applied electric loading makes the crack opening smaller.

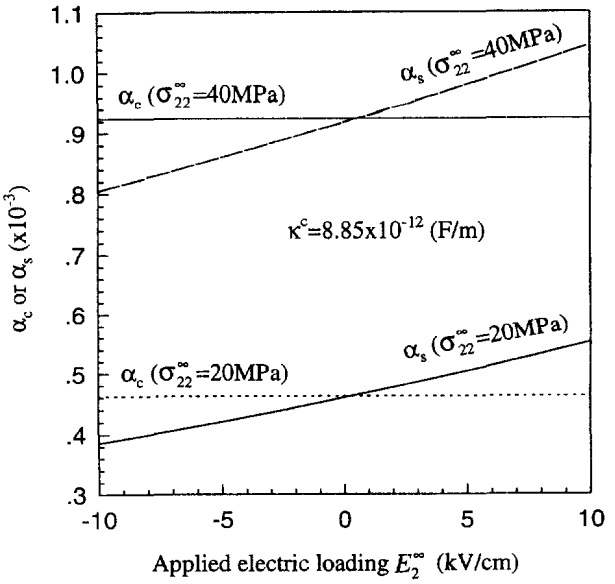

Fig. 11. Comparison of a self-consistent calculation with a conventional calculation for crack deformation under combined mechanical and electric loadings.

Since the geometry of a crack affects its propagation, the deformed crack profile should be used in the calculation of the energy release rate. Figure 12 shows the energy release rate calculated using the deformed crack profile α_s. Since both the magnitude and the change of α_s are very small in the loading range, the energy release rate is almost symmetric about $E_2^{\infty} = 0$ when the crack medium is considered as a vacuum ($\kappa^c = 8.85 \times 10^{-12}$ F/m). If the applied electric loading is much larger, the influence of α_s would be emerged and the energy release rate would be expected to be asymmetric. For a vacuum crack $\kappa^c = 8.85 \times 10^{-12}$ (F/m) and the applied electric field E_2^{∞} contributes nothings to the energy release rate if the electric field inside the crack is taken into account and if the crack undeformed profile is used. Using the self-consistent calculation, we can determine the crack opening and then calculate the energy release rate by eqn (54). Figure 13 compares the energy release rates obtained from the three calculations: (1) counting the electric field inside the crack and using the undeformed crack profile; (2) counting the electric field inside the crack and using the deformed crack profile (the self-consistent calculation); and (3) ignoring the electric

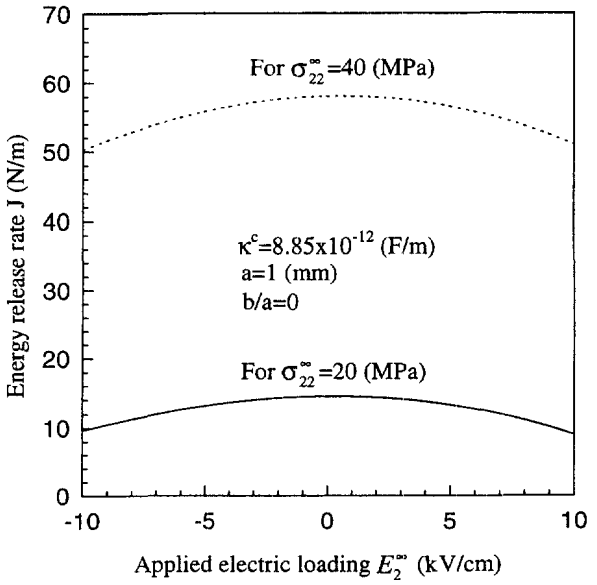

Fig. 12. Energy release rate as a function of applied electric loading using the crack profile calculated by the self-consistent method.

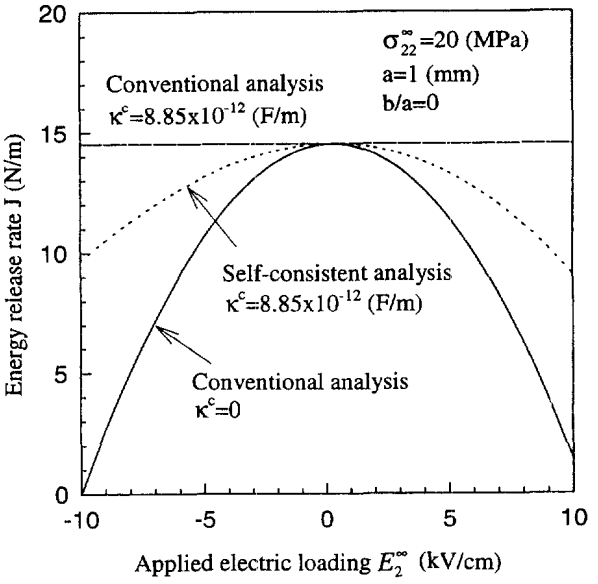

Fig. 13. Comparison of the self-consistent calculation with the conventional calculations for energy release rate.

field inside the crack and using the undeformed crack profile. Ignoring the electric field inside the crack means taking the dielectric constant $\kappa^c = 0$. As can be seen in Fig. 13 that using the self-consistent calculation, the applied electric field E_2^{∞} produce also a resistance to crack propagation, but the resistance is much smaller than that obtained from ignoring the electric field inside the crack.

For a given piezoelectric material, the fracture toughness should be a constant. When the energy release rate is larger than the fracture toughness the crack will propagate. As illustrated in Fig. 13 that the electric field E_2^{∞} may be against the mechanical loadings to propagate the crack. In other words, the critical mechanical loading may be enhanced by an applied electric field. In Fig. 14 the energy release rate is fixed as the same as that under pure mechanical loading, $\sigma_{22}^{\infty} = 20$ MPa. As expected, the applied mechanical loading maintains if the electric field inside the crack is taken into account and the undeformed crack profile is used. For the other two cases, either a positive or a negative applied electric field along the x_2-axis requests a higher mechanical loading to propagate the crack

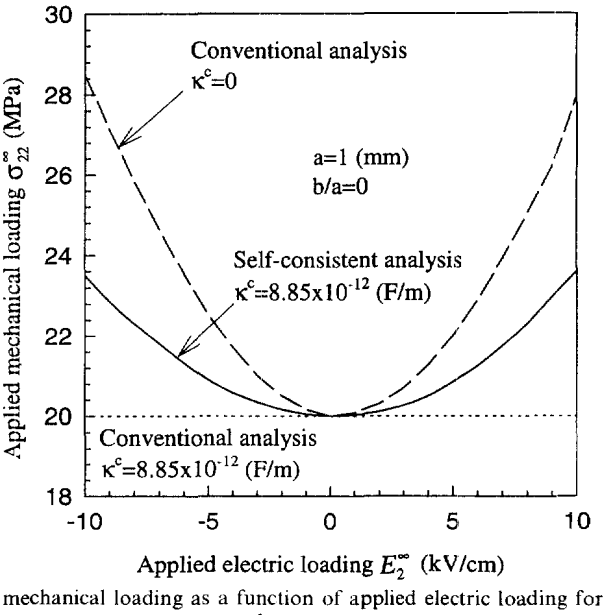

Fig. 14. Applied mechanical loading as a function of applied electric loading for a given energy release rate.

propagation. Again, the conventional calculation (ignoring the electric field inside the crack and using the undeformed crack profile) leads to a higher level of mechanical loading than that obtained from the self-consistent calculation.

For a conductive crack, the results of crack deformation and energy release rate evaluated from the self-consistent calculation are nearly the same as those obtained from the conventional calculation since there is no electric field inside the crack. It should be pointed out again that an applied electric field parallel to the crack can promote crack propagation mainly due to the electrostrictive effects.

7. CONCLUDING REMARKS

This paper presents analytical solutions with finite element confirmation for an infinite piezoelectric medium with an elliptical cavity or a slit crack under combined mechanical–electrical loadings. The effects of electric loadings on the energy release rate of the crack or cavity have been studied. The results show that a complex four-dimensional vector of intensity factors is needed to describe the crack tip stress and electric fields in the linear electric–elastic analysis. The first three components of the vector are real and correspondingly equal to the half values of the mode II, I and III stress intensity factors. The fourth component of the complex vector is real for an insulating crack and, in general, complex for a conducting crack. The electric displacement intensity factor has the conventional form when the parameter d equals zero which requires that the ratio of the dielectric constant of the crack to the effective dielectric constant of the material is much smaller than the ratio of the minor semi-axis to the major semi-axis of the ellipse. It is difficult to meet this requirement in real piezoelectric materials. The electric field inside the cavity is uniform and depends on the combined applied mechanical and electrical loadings, the electric property of the cavity and the ratio of the minor semi-axis to the major semi-axis. For a slit vacuumed crack, the electric field inside the crack in the direction perpendicular to the crack magnifies the corresponding electric loading by more than 1000 times. In the presence of such a strong electric field inside the crack, the self-consistent analysis is needed to determine the deformed crack profile and the energy release rate for crack propagation. In addition, the high electric field inside the crack may cause electric-breakdown, which will change the insulating crack to a conducting one.

The energy release rate for the propagation of an elliptical cavity with a constant ratio of the minor semi-axis to the major semi-axis is a function of the combined mechanical–electrical loadings, the ellipse geometry and the dielectric constant of the cavity medium. For an insulating crack, the energy release rate is independent of the applied electric field either perpendicular or parallel to the crack when the electric field inside the crack is taken into account. For a conducting crack, even though the electric field perpendicular to the crack does not contribute to the energy release rate, the applied electric field parallel to the crack drives the crack to propagate. Makino and Kamiya (1994) investigated experimentally the effects of applied electric field on the modulus of rupture (fracture strength). Their results show that either a positive or a negative electric field reduces the modulus of rupture. We have comprehensively studied the effects of applied electric field on the modulus of rupture and observed the similar phenomenon (Fu and Zhang, 1997a). The original insulating crack may breakdown electrically and cause a fundamental change in its behavior. The detailed results will be reported separately (Fu and Zhang, 1997b).

Acknowledgements—The authors thank Professor Huajian Gao from Stanford University for useful discussions. Financial support from the Hong Kong Research Grants Council under RGC grant HKUST573/94E is gratefully acknowledged.

REFERENCES

Barnett, D. M. and Lothe, J. (1975) Dislocations and line charges in anisotropic piezoelectric insulators. *Physics and State Solids* (*b*) **67**, 105–111.

Cao, H. and Evans, A. G. (1993) Nonlinear deformation of ferroelectric ceramics. *Journal of American Ceramic Society* **76**, 890–896.

Cherepanov, G. P. (1979) *Mechanics of Brittle Fracture*. McGraw-Hill, New York, pp. 317–341.
Deeg, W. F. J. (1980) The analysis of dislocation, crack, and inclusion problems in piezoelectric solids. Ph.D. thesis, Stanford University.
Dunn, M. L. (1994) The effects of crack face boundary conditions on the fracture mechanics of piezoelectric solids. *Engineering Fracture Mechanics* **48,** 25–39.
Eshelby, J. D., Read, W. T. and Shockley, W. (1953) Anisotropic elasticity with applications to dislocation theory. *Acta Metallurgica* **1,** 251–259.
Fu, R. and Zhang, T.-Y. (1997a) Effects of an applied electric field on the modulus of rupture of poled PZT ceramics. *Journal of American Ceramic Society* (in press).
Fu, R. and Zhang, T.-Y. (1997b) Electric-breakdown model for fracture of piezoelectric ceramics (unpublished work).
Gao, H., Zhang, T.-Y. and Tong, P. (1997) Local and global energy release rates for an electrically yield crack in piezoelectric ceramics. *Journal of Mechanics and Physics of Solids* **45,** 491–510.
Hom, C. L., Brown, S. A. and Shankar, N. (1996) Constitutive and failure models for relaxor ferroelectric ceramics. *Proceedings of Smart Structures and Materials* 1966: *Mathematics and Control in Smart Structures* (eds) V. V. Varadan and J. Chandra, **2715,** 316–328.
Jona, F. and Shirane, G. (1993) *Ferroelectric Crystals*. Dover Publications, New York.
Kumar, S. and Singh, R. N. (1996) Crack propagation in piezoelectric materials under combined mechanical and electrical loadings. *Acta Materiala* **44,** 173–200.
Kumar, S. and Singh, R. N. (1997a) Energy release rate and crack propagation in piezoelectric materials. Part I: mechanical/electrical load. *Acta Materiala* **44,** 849–857.
Kumar, S. and Singh, R. N. (1997b) Energy release rate and crack propagation in piezoelectric materials. Part II: combined mechanical and electrical loads. *Acta Materiala* **44,** 859–868.
Lothe, J. and Barnett, D. M. (1975) Integral formalism for surface waves in piezoelectric crystals. Existence considerations. *Journal of Applied Physics* **47,** 1799–1807.
Lynch, C. S. (1996a) Residual stress contribution to fracture of ferroelectric ceramics. *Proceedings of Smart Structures and Materials* 1996: *Mathematics and Control in Smart Structures* (eds) V. V. Varadan and J. Chandra, **2715,** 359–365.
Lynch, C. S. (1996b) The effect of uniaxial stress on the electro-mechanical response of 8/65/35 PLZT. *Acta Materiala* **44,** 4137–4148.
Makino, H. and Kmiya, N. (1994) Effects of dc electric field on mechanical properties of piezoelectric ceramics. *Japanese Journal of Applies Physics* **33,** 5323–5327.
McMeeking, R. M. (1989) Electrostrictive stresses near crack-like flaws. *Journal of Applied Mathematics and Physics* **40,** 615–627.
McMeeking, R. M. (1987) On mechanical stresses at cracks in dielectrics with application to dielectric breakdown. *Journal of Applied Physics* **62,** 3116–3122.
Mehta, K. and Virkar, A. V. (1990) Fracture mechanisms in ferroelectric–ferroelastic lead zirconate titanate (Zr: Ti = 0.54: 0.46) ceramics. *Journal of American Ceramic Society* **73,** 567–574.
Mikahailov, G. K. and Parton, V. Z. (1990) *Electromagnetoelasticity*. Hemisphere, New York.
Pak, Y. E. and Herrmann, G. (1986) Conservation laws and the material momentum tensor for the elastic dielectric. *International Journal of Engineering Science* **24,** 1365–1374.
Pak, Y. E. (1990) Crack extension force in a piezoelectrical material. *Journal of Applied Mechanics* **57,** 647–653.
Pak, Y. E. (1992) Linear electro-elastic fracture mechanics of piezoelectric materials. *International Journal of Fracture* **54,** 79–100.
Pak, Y. E. and Tobin, A. (1993) On electric field effects in fracture of piezoelectric materials. *Mechanical and Electromagnetic Material Structures* **AMD 161/MD 42,** 51–62.
Park, S. and Sun, C.-T. (1995) Fracture criteria for piezoelectric ceramics. *Journal of American Ceramic Society* **78,** 1475–1480.
Parton, V. Z. and Kudryavtsev, B. A. (1988) *Electromagnetoelasticity Piezoelectrics and Electrically Conductive Solids*. Gordon and Breach Science Publishers, New York.
Pohanka, R. C., Rice, R. W. and Walker, B. E. Jr (1976) Effect of internal stress on the strength of $BaTiO_3$. *Journal of American Ceramic Society* **59,** 71–74.
Pohanka, R. C., Freiman, S. W. and Bender, B. A. (1978) Effect of phase transformation on the fracture behaviour of $BaTiO_3$. *Journal of American Ceramic Society* **61,** 72–75.
Rice, J. R. (1968) Mathematical analysis in the mechanics of fracture. *Fracture*, Vol. II (ed. H. Liebowitz), pp. 191–311. Academic Press, New York.
Sosa, H. and Pak, Y. E. (1990) Three-dimensional eigenfunction analysis of a crack in a piezoelectric material. *International Journal of Solids and Structures* **26,** 1–15.
Sosa, H. (1991) Plane problems in piezoelectric media with defects. *International Journal of Solids and Structures* **28,** 491–505.
Sosa, H. (1992) On the fracture mechanics of piezoelectric solids. *International Journal of Solids and Structures* **29,** 2613–2622.
Stroh, A. N. (1958) Dislocations and crack in anisotropic elasticity. *Philosophical Magazine* **3,** 625–646.
Suo, Z., Kuo, C. M., Barnett, D. M. and Willis, J. R. (1992) Fracture mechanics for piezoelectric ceramics. *Journal of Mechanics and Physics of Solids* **40,** 739–765.
Suo, Z. (1993) Models for breakdown-resistant dielectric and ferroelectric ceramics. *Journal of Mechanics and Physics of Solids* **41,** 1155–1176.
Ting, T. C. T. (1996) *Anisotropic Elasticity: Theory and Applications*. Oxford University Press, New York.
Tobin, A. G. and Pak, Y. E. (1993) Effect of electric fields on fracture behavior of PZT ceramics. *Proceedings of the* 1993 *North American Conference on Smart Structures and Materials: Smart Materials* (ed.) V. K. Varadan, **1916,** 78–86.
Yamamoto, T., Igarashi, H. and Okazaki, K. (1983) Internal stress anisotropies induced by electric field in Lanthanum modified $PbTiO_3$ ceramics. *Ferroelectrics* **50,** 273–278.
Zhang, T. Y. and Hack, J. E. (1992) Mode-III cracks in piezoelectric materials. *Journal of Applied Physics* **71,** 5865–5870.

Zhang, T. Y. (1994a) Effect of sample width on the energy release rate and electric boundary conditions along crack surfaces in piezoelectric materials. *International Journal of Fracture* **66,** R33–R38.
Zhang, T. Y. (1994b) J-integral measurement for piezoelectric materials. *International Journal of Fracture* **68,** R33–R40.
Zhang, T. Y. and Tong, P. (1996) Fracture mechanics for a mode-III crack in a piezoelectric material. *International Journal of Solids and Structures* **33,** 343–359.

APPENDIX 1

General solution

Barnett and Lothe (1975), Suo *et al.* (1992), Sosa and Pak (1990), Pak (1992) and Park (1994) have formulated the general solution using Stroh formalism (Eshelby *et al.*, 1953; Stroh, 1958; Ting, 1996) with strains and electric field strengths which, in turn, can be expressed in terms of the displacements and electric potential, as independent variables. In this case, the governing equations are given by:

$$\varepsilon_{ij} = \tfrac{1}{2}(u_{i,j} + u_{j,i}), \quad E_i = -\phi_{,i}$$
$$\sigma_{ij,j} = 0, \quad D_{i,i} = 0 \tag{A1}$$

with boundary conditions

$$\sigma \cdot \mathbf{n} = \mathbf{t}$$
$$(\mathbf{D}^1 - \mathbf{D}^2) \cdot \mathbf{n} = -q$$
$$(\mathbf{E}^1 - \mathbf{E}^2) \times \mathbf{n} = 0 \tag{A2}$$

where u_i is a component of the displacement vector, ϕ is the electric potential, q is the density of free charge on the surface between the two media, $\mathbf{t}$ is the traction along the boundary, and $\mathbf{n}$ is the unit vector normal to the boundary.

Following Barnett and Lothe's (1975) treatment, the three-dimensional space is extended to a four-dimensional space in the following steps:

(1) define a new operator

$$\frac{\partial}{\partial x_4} \equiv 0 \tag{A3}$$

(2) let u_4 denote the electric potential ϕ
(3) define new strain components

$$S_{ij} = \varepsilon_{ij}$$
$$S_{i4} = S_{4i} = -\tfrac{1}{2}E_i \quad \text{and} \quad S_{44} = 0 \quad i,j = 1,2,3 \tag{A4}$$

(4) define new stress components

$$\Sigma_{ij} = \sigma_{ij}$$
$$\Sigma_{i4} = \Sigma_{4i} = D_i \quad \text{and} \quad \Sigma_{44} = 0 \quad i,j = 1,2,3 \tag{A5}$$

(5) define new elastic constant components

$$C_{ijkl} = c^{E}_{ijkl}$$
$$C_{4kl4} = C_{4k4l} = C_{k44l} = C_{k4l4} = -\kappa^{e}_{kl}$$
$$C_{4jkl} = C_{j4kl} = C_{kl4j} = C_{klj4} = e_{jkl}, \quad i,j,k,l = 1,2,3$$
$$C_{44kl} = C_{kl44} = C_{j444} = C_{4j44} = C_{44j4} = C_{444j} = C_{4444} = 0. \tag{A6}$$

The extended elastic constant tensor is still symmetric

$$C_{ijkl} = C_{klij} = C_{jikl} = C_{ijlk}. \tag{A7}$$

Consequently, the governing and constitutive equations can be expressed in the four-dimensional system as

$$S_{ij} = \tfrac{1}{2}(u_{i,j} + u_{j,i})$$
$$\Sigma_{ij} = C_{ijkl}S_{kl}$$
$$\Sigma_{ij,j} = 0, \quad i,j,k,l = 1,2,3,4. \tag{A8}$$

Thereafter, a repeated subscript denotes summation from 1 to 4 unless specified otherwise.

When u_i are functions of x_1 and x_2 only, the general solution is given by

$$u_i = A_i f(z) \tag{A9}$$

where

$$z = x_1 + p x_2. \tag{A10}$$

Combining eqns (A8) and (A9), we have

$$[\mathbf{Q} + (\mathbf{R} + \mathbf{R}^{\mathrm{T}})p + \mathbf{T}p^2]A_i = 0 \tag{A11}$$

where

$$Q_{ij} = C_{i1k1}, \quad R_{ik} = C_{i1k2} \quad \text{and} \quad T_{ik} = C_{i2k2}. \tag{A12}$$

A non-zero solution of A_k requires that

$$\det[\mathbf{Q} + (\mathbf{R} + \mathbf{R}^{\mathrm{T}})p + \mathbf{T}p^2] = 0. \tag{A13}$$

Equation (A13) has eight roots which cannot be real because of the positive definiteness of the strain energy and electric energy densities. The eight roots form four conjugate pairs and we shall choose $\mathrm{Im}(p_\alpha) > 0$ for $\alpha = 1, 2, 3, 4$.

In general, the extended displacements and stresses can be represented as

$$\mathbf{u} = \mathbf{A}\mathbf{f}(z) + \overline{\mathbf{A}\mathbf{f}(z)} \tag{A14}$$

$$\Sigma_2 = \psi_{,1} \quad \text{and} \quad \Sigma_1 = -\psi_{,2} \tag{A15}$$

$$\psi = \mathbf{L}\mathbf{f}(z) + \overline{\mathbf{L}\mathbf{f}(z)}. \tag{A16}$$

The matrices **A** and **L** have the following correlation

$$\mathbf{L} = (\mathbf{R}^{\mathrm{T}} + p\mathbf{T})\mathbf{A} = -\frac{1}{p}(\mathbf{Q} + p\mathbf{R})\mathbf{A}. \tag{A17}$$

Equation (A17) can be rearranged into a standard eigen-equation

$$\mathbf{N}\zeta_\alpha = p_\alpha \zeta_\alpha$$

$$\mathbf{N} = \begin{pmatrix} \mathbf{N}_1 & \mathbf{N}_2 \\ \mathbf{N}_3 & \mathbf{N}_1^{\mathrm{T}} \end{pmatrix}, \quad \zeta = \begin{pmatrix} \mathbf{A} \\ \mathbf{L} \end{pmatrix}$$

$$\mathbf{N}_1 = -\mathbf{T}^{-1}\mathbf{R}^{\mathrm{T}}, \quad \mathbf{N}_2 = \mathbf{T}^{-1} = \mathbf{N}_2^{\mathrm{T}}, \quad \mathbf{N}_3 = \mathbf{R}\mathbf{T}^{-1}\mathbf{R}^{\mathrm{T}} - \mathbf{Q} = \mathbf{N}_3^{\mathrm{T}}. \tag{A18}$$

Since the eigen-vectors are uniquely determined up to an arbitrary multiplicative constant, they are normalized to meet the properties:

$$\mathbf{A}\mathbf{A}^{\mathrm{T}} + \overline{\mathbf{A}\mathbf{A}^{\mathrm{T}}} = \mathbf{L}\mathbf{L}^{\mathrm{T}} + \overline{\mathbf{L}\mathbf{L}^{\mathrm{T}}} = 0$$

$$\mathbf{L}\mathbf{A}^{\mathrm{T}} + \overline{\mathbf{L}\mathbf{A}^{\mathrm{T}}} = \mathbf{A}\mathbf{L}^{\mathrm{T}} + \overline{\mathbf{A}\mathbf{L}^{\mathrm{T}}} = \mathbf{I} \tag{A19}$$

where **I** is the identity matrix. Now, the mechanical and electrical coupling problem is reduced to the standard eigen-equation (A18). Moreover, the matrix **B**,

$$\mathbf{B} = i\mathbf{A}\mathbf{L}^{-1} \tag{A20}$$

is a Hermitian matrix and can be divided into

$$\mathbf{B} = \begin{pmatrix} \mathbf{B}_1 & \mathbf{B}_2 \\ \mathbf{B}_3 & \mathbf{B}_{44} \end{pmatrix} \tag{A21}$$

where $\mathbf{B}_1$ is the 3×3 upper left-hand block and B_{44} is the lower right-hand element. For stable materials Lothe and Barnett (1975) show that

$$\mathbf{B}_2 = \bar{\mathbf{B}}_3^{\mathrm{T}}, \quad \mathbf{B}_1 \text{ is positive definite, but } B_{44} < 0. \tag{A22}$$

APPENDIX 2

Thermodynamic functions and the energy release rate

Parton and Kudryavtsev (1988) summarized the thermodynamic functions for piezoelectric materials. The internal energy, electric enthalpy and full Gibbs energy are briefly described here. The internal energy per unit volume, u is expressed in a differential form as

$$\mathrm{d}u = \sigma_{ij}\,\mathrm{d}\varepsilon_{ij} + E_i\,\mathrm{d}D_i + T\,\mathrm{d}s \tag{A23}$$

where s is the entropy per unit volume; T is the absolute temperature; $\mathbf{E}$ and $\mathbf{D}$ are the electric field strength and electric displacement vectors, respectively; and σ_{ij}, and ε_{ij} are the components of stress and strain tensors, respectively. Define the free energy per unit volume, f as

$$f = u - Ts \tag{A24}$$

for which

$$\mathrm{d}f = \sigma_{ij}\,\mathrm{d}\varepsilon_{ij} + E_i\,\mathrm{d}D_i - s\,\mathrm{d}T. \tag{A25}$$

The electric enthalpy per unit volume, h is defined as

$$h = u - E_iD_i - Ts \tag{A26}$$

for which

$$\mathrm{d}h = \sigma_{ij}\,\mathrm{d}\varepsilon_{ij} - D_i\,\mathrm{d}E_i - s\,\mathrm{d}T. \tag{A27}$$

Introduce the mechanical enthalpy per unit volume, w, as

$$w = u - \sigma_{ij}\varepsilon_{ij} - Ts \tag{A28}$$

for which

$$\mathrm{d}w = -\varepsilon_{ij}\,\mathrm{d}\sigma_{ij} + E_i\,\mathrm{d}D_i - s\,\mathrm{d}T. \tag{A29}$$

The full Gibbs function per unit volume, g is defined as

$$g = u - \sigma_{ij}\varepsilon_{ij} - E_iD_i - Ts \tag{A30}$$

for which

$$\mathrm{d}g = -\varepsilon_{ij}\,\mathrm{d}\sigma_{ij} - D_i\,\mathrm{d}E_i - s\,\mathrm{d}T. \tag{A31}$$

At a constant temperature, eqns (A25), (A27), (A29) and (A31) reduce, respectively, to

$$\mathrm{d}f = \sigma_{ij}\,\mathrm{d}\varepsilon_{ij} + E_i\,\mathrm{d}D_i \tag{A32}$$

$$\mathrm{d}h = \sigma_{ij}\,\mathrm{d}\varepsilon_{ij} - D_i\,\mathrm{d}E_i \tag{A33}$$

$$\mathrm{d}w = -\varepsilon_{ij}\,\mathrm{d}\sigma_{ij} + E_i\,\mathrm{d}D_i \tag{A34}$$

$$\mathrm{d}g = -\varepsilon_{ij}\,\mathrm{d}\sigma_{ij} - D_i\,\mathrm{d}E_i. \tag{A35}$$

There are two independent variables, one is mechanical and the other is electrical, determining the four thermodynamic functions at a constant temperature. The independent mechanical variable can be the strains or the stresses, while the independent electric variable can be the electric field strengths or the electric displacements. If the strains and the electric field strengths are considered as independent variables, the stresses and electric displacements are given by

$$\begin{aligned}\sigma_{ij} &= c^{\mathrm{E}}_{ijkl}\varepsilon_{kl} - e_{kij}E_k\\ D_i &= e_{ikl}\varepsilon_{kl} + \kappa^{\varepsilon}_{ik}E_k\end{aligned} \tag{A36}$$

where c^{E}_{klij} are the isothermal elastic constants, e_{mij} are the piezoelectric constants, and $\kappa^{\varepsilon}_{ik}$ are the isothermal dielectric constants at constant strains. Equation (A36) expresses the linear relationship among the four variables. If another two variables are treated as independent variables, the corresponding constitutive equations can be obtained by re-arranging eqn (A36). For example, if the independent variables are the stresses and the electric field strengths, the constitution equations are given by

$$\begin{aligned}\varepsilon_{ij} &= s^{\mathrm{E}}_{ijkl}\sigma_{kl} + d^{\mathrm{p}}_{kij}E_k\\ D_i &= d^{\mathrm{p}}_{kij}\sigma_{kl} + \kappa^{\sigma}_{ik}E_k\end{aligned} \tag{A37}$$

where s^{E}_{ijkl} are the isothermal elastic compliancies at a constant electric field strength; κ^{σ}_{ik} are the isothermal dielectric permittivities at constant stresses; d^{p}_{kij} are the piezoelectric moduli. There are relations among these material properties:

$$\begin{aligned}(\mathbf{s}^{\mathrm{E}})^{-1} &= \mathbf{c}^{\mathrm{E}}\\ \mathbf{d}^{\mathrm{p}} &= \mathbf{e}\mathbf{s}^{\mathrm{E}}, \quad \mathbf{e} = \mathbf{d}^{\mathrm{p}}\mathbf{c}^{\mathrm{E}}\\ \kappa^{\sigma} &= \kappa^{\varepsilon} - \mathbf{d}^{\mathrm{p}}\mathbf{e}.\end{aligned} \tag{A38}$$

From eqns (A32)–(A35), we have the following statements of the total virtual work for the entire domain, Π, for an isothermal process

$$\int_\Gamma (t_i\,\delta u_i - \phi n_i\,\delta D_i)\,\mathrm{d}\Gamma - \int_\Pi \delta f\,\mathrm{d}\Pi = 0 \tag{A39}$$

$$\int_\Gamma (t_i\,\delta u_i + D_i\,\delta\phi n_i)\,\mathrm{d}\Gamma - \int_\Pi \delta h\,\mathrm{d}\Pi = 0 \tag{A40}$$

$$\int_\Gamma (-u_i\,\delta t_i - \phi n_i D_i\,\delta D_i)\,\mathrm{d}\Gamma - \int_\Pi \delta w\,\mathrm{d}\Pi = 0 \tag{A41}$$

$$\int_\Gamma (-u_i\,\delta t_i + D_i\,\delta\phi n_i)\,\mathrm{d}\Gamma - \int_\Pi \delta g\,\mathrm{d}\Pi = 0 \tag{A42}$$

where Γ denotes the boundary of the domain, u_i is a component of the displacement vector, ϕ is the electric potential, $\mathbf{t}$ is the traction along the boundary, and $\mathbf{n}$ is the unit vector normal to the boundary. Equation (A42) was derived before by Zhang (1994b). Introducing four isothermal potential energies as

$$P_F = \int_\Gamma (t_i u_i - D_i\phi n_i)\,\mathrm{d}\Gamma - \int_\Pi f\,\mathrm{d}\Pi \tag{A43}$$

where the prescribed properties on the boundary are stresses and electric potential;

$$P_H = \int_\Gamma (t_i u_i + D_i\phi n_i)\,\mathrm{d}\Gamma - \int_\Pi h\,\mathrm{d}\Pi \tag{A44}$$

where the prescribed properties on the boundary are stresses and electric displacements;

$$P_W = \int_\Gamma (-u_i t_i - D_i\phi n_i)\,\mathrm{d}\Gamma - \int_\Pi w\,\mathrm{d}\Pi \tag{A45}$$

where the prescribed properties on the boundary are displacements and electric potential:

$$P_G = \int_\Gamma (-u_i t_i + D_i\phi n_i)\,\mathrm{d}\Gamma - \int_\Pi g\,\mathrm{d}\Pi \tag{A46}$$

where the prescribed properties on the boundary are displacements and electric displacement.

Thus, eqns (A39)–(A42) can be re-written as

$$\delta P_F = \int_\Gamma (t_i\,\delta u_i - \phi n_i\,\delta D_i)\,\mathrm{d}\Gamma - \int_\Pi \delta f\,\mathrm{d}\Pi = 0 \tag{A47}$$

$$\delta P_H = \int_\Gamma (t_i\,\delta u_i + D_i\,\delta\phi n_i)\,\mathrm{d}\Gamma - \int_\Pi \delta h\,\mathrm{d}\Pi = 0 \tag{A48}$$

$$\delta P_W = \int_\Gamma (-u_i\,\delta t_i - \phi n_i\,\delta D_i)\,\mathrm{d}\Gamma - \int_\Pi \delta w\,\mathrm{d}\Pi = 0 \tag{A49}$$

$$\delta P_G = \int_\Gamma (-u_i\,\delta t_i + D_i\,\delta\phi n_i)\,\mathrm{d}\Gamma - \int_\Pi \delta g\,\mathrm{d}\Pi = 0. \tag{A50}$$

If the generalized force, P, the generalized displacement, Δ, the generalized voltage, V and the generalized charge, Q are used, then the changes in the total free energy, F, the total electric enthalpy, H, the total mechanical enthalpy, W and the total full Gibbs energy, G for the entire sample are given by

$$\mathrm{d}F = P\,\mathrm{d}\Delta + V\,\mathrm{d}Q \tag{A51}$$

$$\mathrm{d}H = P\,\mathrm{d}\Delta - Q\,\mathrm{d}V \tag{A52}$$

$$\mathrm{d}W = -\Delta\,\mathrm{d}P + V\,\mathrm{d}Q \tag{A53}$$

$$\mathrm{d}G = -\Delta\,\mathrm{d}P - Q\,\mathrm{d}V. \tag{A54}$$

Now, consider a piezoelectric material containing a pre-crack. Adding the energy change associated with the crack extension into each of eqns (A51)–(A54) leads to

$$dF = P d\Delta + V dQ - J dA \tag{A55}$$

$$dH = P d\Delta - Q dV - J dA \tag{A56}$$

$$dW = -\Delta dP + V dQ - J dA \tag{A57}$$

$$dG = -\Delta dP - Q dV - J dA \tag{A58}$$

where A is the crack area; and J is the energy release rate for crack propagation and defined as

$$J = -\left(\frac{\partial F}{\partial A}\right)_{\Delta,Q} = -\left(\frac{\partial H}{\partial A}\right)_{\Delta,V} = -\left(\frac{\partial W}{\partial A}\right)_{P,Q} = -\left(\frac{\partial G}{\partial A}\right)_{P,V}. \tag{A59}$$

Alternatively, the energy release rate can be evaluated by following Rice's (1968) treatment of elastic fracture mechanics and is given by†

$$J = \frac{\partial P_{\mathrm{F}}}{\partial A} = \frac{\partial P_{\mathrm{H}}}{\partial A} = \frac{\partial P_{\mathrm{W}}}{\partial A} = \frac{\partial P_{\mathrm{G}}}{\partial A}. \tag{A60}$$

APPENDIX 3

N matrix for the x_2*-axis in the poling direction*

When the x_2-axis is chosen to be parallel to the poling direction, the extended constitute equation is given by eqn (A8). Consequently, the **Q**, **R** and **T** matrices have, respectively, the following forms:

$$\mathbf{Q} = \begin{bmatrix} c_{11} & 0 & 0 & 0 \\ 0 & c_{44} & 0 & e_{15} \\ 0 & 0 & \dfrac{c_{11}-c_{12}}{2} & 0 \\ 0 & e_{15} & 0 & -\kappa_{11} \end{bmatrix}$$

$$\mathbf{R} = \begin{bmatrix} 0 & c_{13} & 0 & e_{31} \\ c_{44} & 0 & 0 & 0 \\ 0 & 0 & 0 & 0 \\ e_{15} & 0 & 0 & 0 \end{bmatrix}$$

$$\mathbf{T} = \begin{bmatrix} c_{44} & 0 & 0 & 0 \\ 0 & c_{33} & 0 & e_{33} \\ 0 & 0 & c_{44} & 0 \\ 0 & e_{33} & 0 & -\kappa_{33} \end{bmatrix}. \tag{A62}$$

Thus, the **N** matrix is obtained as

$$\mathbf{N} = \begin{bmatrix} 0 & -1 & 0 & -\dfrac{e_{15}}{c_{44}} & \dfrac{1}{c_{44}} & 0 & 0 & 0 \\ N_{21} & 0 & 0 & 0 & 0 & N_{26} & 0 & N_{28} \\ 0 & 0 & 0 & 0 & 0 & 0 & \dfrac{1}{c_{44}} & 0 \\ N_{41} & 0 & 0 & 0 & 0 & N_{28} & 0 & N_{48} \\ N_{51} & 0 & 0 & 0 & 0 & N_{21} & 0 & N_{41} \\ 0 & 0 & 0 & 0 & -1 & 0 & 0 & 0 \\ 0 & 0 & \dfrac{c_{12}-c_{11}}{2} & 0 & 0 & 0 & 0 & 0 \\ 0 & 0 & 0 & \dfrac{e_{15}^2}{c_{44}}+\kappa_{11} & -\dfrac{e_{15}}{c_{44}} & 0 & 0 & 0 \end{bmatrix} \tag{A63}$$

where

† In the previous work (Zhang and Tong, 1996) the contribution to the energy release rate from the boundary integrals, as shown in eqns (A47)–(A50), was not taken into account. The sign of the electric terms in eqns (58), (59), (71), (74) and (75) in the previous work should be changed from plus to minus.

$$N_{21} = -\frac{\kappa_{33}c_{13}+e_{33}e_{31}}{\tau}, \quad N_{26} = \frac{\kappa_{33}}{\tau}, \quad N_{28} = \frac{e_{33}}{\tau}$$

$$N_{41} = \frac{e_{31}c_{33}-e_{33}c_{13}}{\tau}, \quad N_{48} = -\frac{c_{33}}{\tau}$$

$$N_{51} = \frac{\kappa_{33}c_{13}^2+2c_{13}e_{33}e_{31}-c_{33}e_{31}^2}{\tau} - c_{11}$$

$$\tau = c_{33}\kappa_{33}+e_{33}^2.$$

Then, it is straightforward to solve the standard eigne-equation of eqn (A18) using a commercial code, such as MATLAB.